Earth Systems and Environment (2026) 10:5843–5868
https://doi.org/10.1007/s41748-025-00938-y

ORIGINAL ARTICLE

AI Driven Impact Assessment of Shaheen Tropical Cyclone Using Very High-Resolution Satellite Data

Yaseen Al-Mulla[1,2] · Mohammed Al-Muqaimi[1] · Ahsan Ali[1] · Farid Melgani[3] · Krishna Parimi[1] · Thuwaiba Al-Wahaibi[1]

Received: 29 July 2025 / Revised: 11 October 2025 / Accepted: 3 November 2025 / Published online: 20 November 2025

Abstract

Understanding tropical cyclones (TCs) impact is critical for implementing effective post–cyclone management methods. While previous researches have assessed the effects of TCs in Oman, this study uniquely examines and quantifies the impact of the Shaheen tropical cyclone (STC) using advanced image resolution and analysis, including artificial intelligence in the form of Multiple Deep learning models, as well as using very high-resolution (41 cm) satellite imagery. This study found significant vegetation loss, with 85.8 ha (51.3%) of dense and 153.2 ha (18.9%) of sparse vegetation destroyed in Al–Khabourah. Al–Suwaiq was the most affected wilayat, losing 3160 ha (55.5%) of shrubs and grasses, 1713.9 ha (67.2%) of dense vegetation, and 609.8 ha (16.6%) of sparse vegetation. The cyclone also caused drastic increases in water surface areas, especially in Al–Khabourah by 496.82 ha and Al–Suwaiq by 180.8 ha. Additionally, 32% (42.73 ha) of buildings in Al–Khabourah and 67.5% (6.4 ha) of fishermen's coastal structures were damaged. The deep learning model accurately classified land cover types with high precision (1, 0.93, 0.89, and 0.9 for barren, dense, sparse vegetation, and buildings, respectively) and an overall accuracy of 94%. Digital Elevation Models and Ruggedness Index maps identified flood-prone zones, especially in coastal areas. Ground validation confirmed model performance with an overall accuracy of 94%. This study demonstrates the effective application of artificial intelligence in the form of multiple deep learning techniques for detecting and mapping various objects, including vegetation, buildings, and water bodies, in the aftermath of the impact of TC. These insights can support government agencies and landowners in developing more effective post–cyclone planning and climate resilience strategies, especially in urban and coastal regions.

✉ Yaseen Al-Mulla
yalmula@squ.edu.om

1 Remote Sensing and GIS Research Center, Sultan Qaboos University, Al-Khod Postal Code 123, Sultanate of Oman

2 Department of Soils, Water and Agricultural Engineering, Sultan Qaboos University, Al-Khod Postal Code 123, Sultanate of Oman

3 Department of Information Engineering and Computer Science, University of Trento, Via Sommarive, 9, Trento 38123, Italy

Graphical Abstract

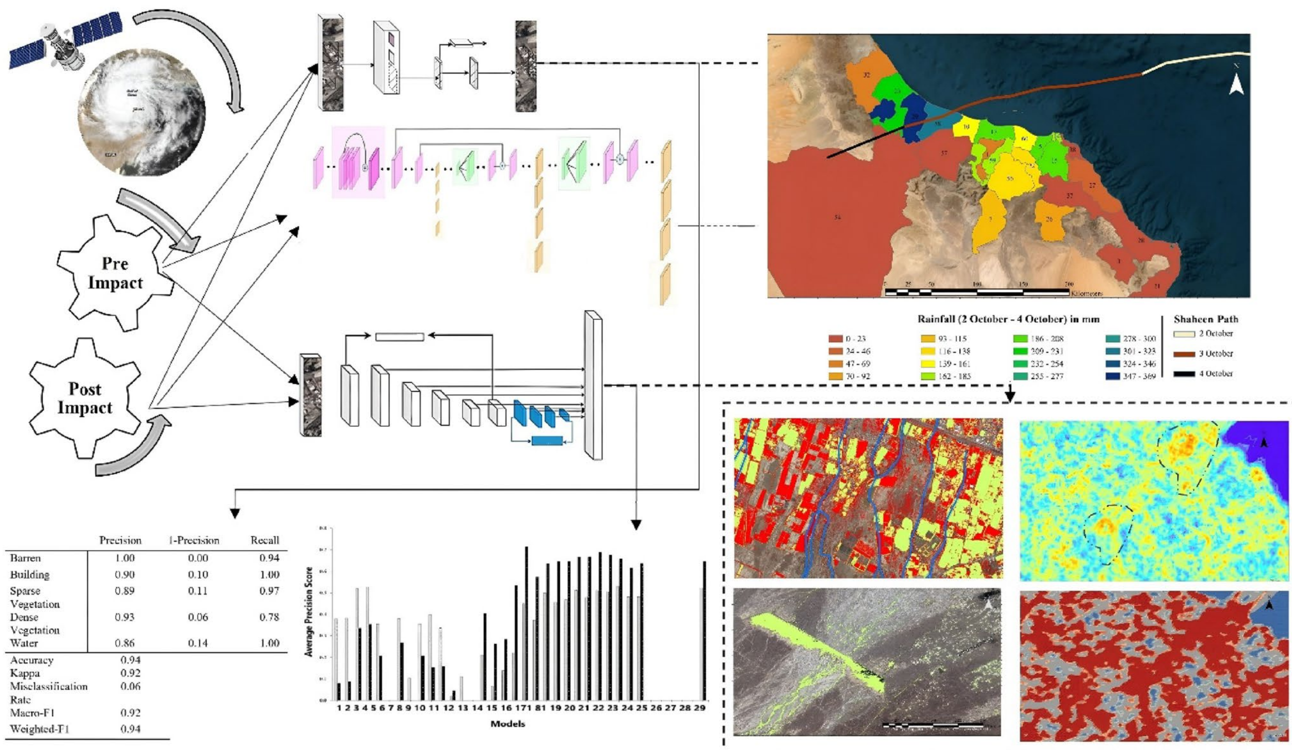

This study used high–resolution satellite imagery to assess the impact of the Shaheen tropical cyclone. The study fused pre–impact and post–impact imagery, which was processed and used to train AI models to detect changes in vegetation, buildings, and water surfaces. The AI models achieved high accuracy (94%), integrating terrain analysis to map flood zones. Results showed severe damage, including a 55.5% loss of shrubs in Al–Suwaiq and 32% building damage in Al–Khabourah. The AI–driven impact assessment offers valuable insights for planning climate resilience to help protect urban areas and biodiversity.

Highlights

- Pre–impact and post–impact satellite imagery was acquired to carry out the impact assessment of Shaheen Tropical Cyclone (STC).
- AI in the form of Multiple Deep learning models was trained with different epochs and applied in the study area using multilayer backbone models.
- Impact assessment of STC was carried out on vegetation, buildings, and water bodies extracted using these models.
- In addition to a drastic increase in water bodies and destruction of vegetation, damage to buildings was also recorded in the study.
- Spatial maps from hot and cold spots analysis and flood inundation analysis were constructed to identify the areas affected in the same scenarios.

Keywords Cyclone damage assessment · Disaster management · Impact assessment · Artificial intelligence · Remote sensing · Deep learning · Change detection · Flood mapping

1 Introduction

Many ecological hindrances are considered challenging for humans, livestock, agriculture, the environment, and infrastructure, while tropical cyclones are one of the most destructive phenomena on the Earth's surface. The intensifying effects of climate change profoundly change both the frequency and intensity of tropical cyclones, which in turn pose a serious threat to the fundamental structure of our ecosystems. This shift has the potential to significantly undermine the essential services these ecosystems deliver, putting at risk the delicate equilibrium of nature that supports all living beings (Kropf et al. 2025). A total of 87 storms were registered and named in the year 2022 around the world (Erick 2025). A criterion is set by the Directorate General of Meteorology in Oman (DGMET), declaring a tropical system as "Tropical Cyclone (TC)" with a maximum sustained wind speed exceeding 63 knots (Al-Zadjali et al. 2021). TCs have a direct impact on the Arabian Peninsula due to their formation in the Indian Ocean as 41 TCs landed in Oman with extreme rainfall, storm surges, and flash floods, causing loss of lives (Al-Manji et al. 2021). Due to its geographical locality and geophysical surroundings, Oman faced direct hits that often influenced and damaged coastal areas (Mansour 2019; Banan-Dallalian et al. 2021).

Since 1970, the severity and incidence of TCs have increased as sea surface temperatures rose (Knutson et al. 2010). Figure 1 shows the occurrence of all TCs in the Arabian Sea recorded by the International Best Track Archive for Climate Stewardship (Gahtan et al. 2024). The Gonu cyclone, the strongest cyclone in the Arabian Sea, impacted the Arabian Peninsula and southern Iran from June 2–7, 2007, killing 49 people in Oman and 23 in Iran (Banan-Dallalian et al. 2021).

TCs have the most significant global impact on coastal areas. Assessment of the overall impacts of TC is crucial for the implementation of effective post–cyclone management strategies (Hoque et al. 2016). The collection of near real-time data, analysis, future prediction, and decision-making is important to mitigate natural disasters caused by TCs. Many sensors must be installed and monitored to collect real-time data. In addition to maintenance and monitoring, many physio-hydrological models have been incorporated to scale the impact of these disasters (Srivastava et al. 2022). However, these traditional methods have proven difficult, time-consuming, and laborious to mitigate the effects of TC and management approaches (Zhang et al. 2013).

In this context, the use of remote sensing has proven to be more accurate and time-saving by adding geospatial analysis and utilizing GIS approaches to alleviate disaster management, including TCs (Cortés-Ramos et al. 2020; Tomaszewski 2020; Hoque et al. 2024; Das and Ghosh 2024). Monitoring and assessing the impact of TCs on socio-environmental aspects using high-resolution satellite imagery is considered crucial for disaster management techniques (Phiri et al. 2020; Behera et al. 2022). There are four main types of hazards caused by TC: destruction caused by strong winds, rainfall flooding, storm surges, and landslides, further causing damage to urban areas, vegetation, beaches, and loss of lives (Murray et al. 2020). Many studies have described the impact of TCs on vegetation (Mandal and Hosaka 2020; Charrua et al. 2021; Kumar et al. 2021;

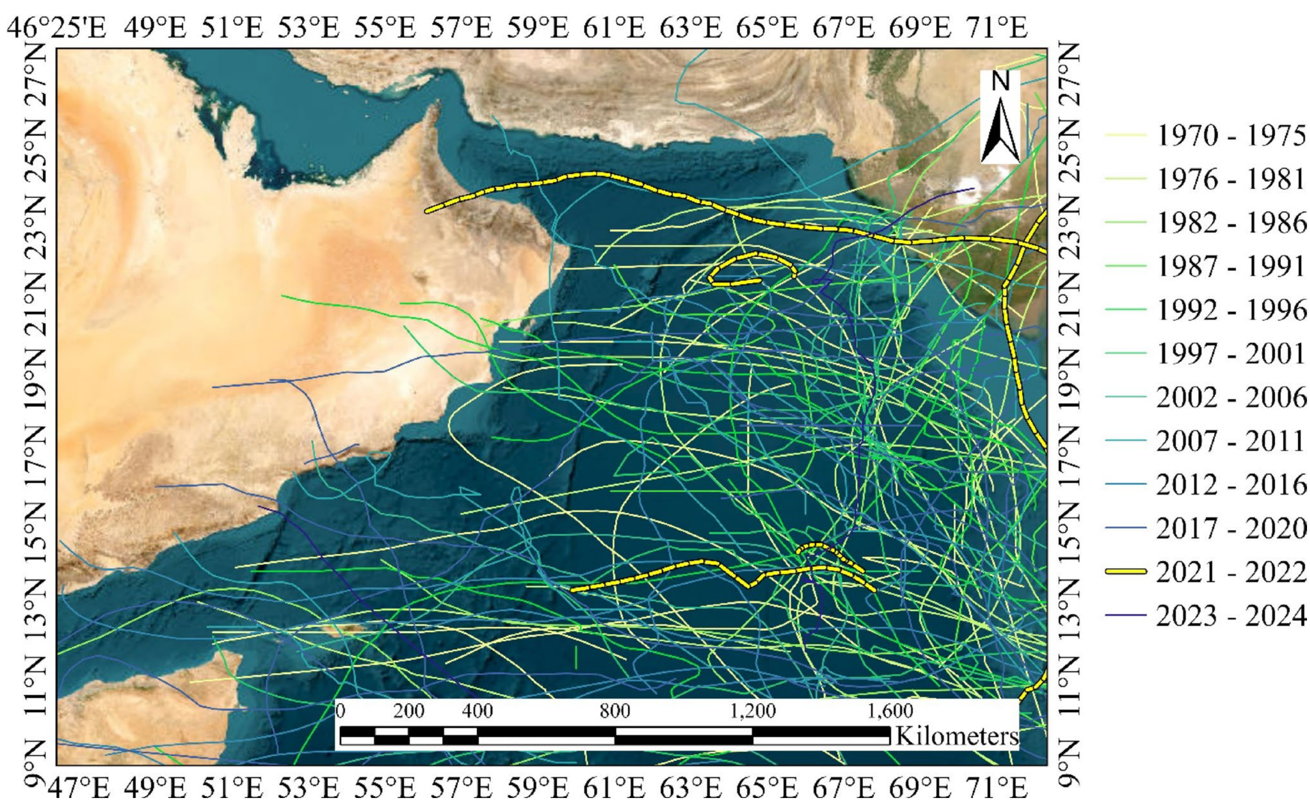

Fig. 1 Occurrence and track record of all tropical storms in the Arabian Sea since 1970 (Gahtan et al. 2024)

Delaporte et al. 2022), urbanization (Fisker et al. 2021), and sea levels (Ningsih et al. 2020).

The addition of deep learning techniques using satellite imagery has helped researchers acquire more accurate results (Feng et al. 2021). Deep learning has been previously used in TC size estimation (Zhuo and Tan 2021; Baek et al. 2022), impact assessment (Berezina and Liu 2022; Nasrin et al. 2023; Maha Arachchige and Pardhan 2025), intensity (Zhang et al. 2021; Jiang et al. 2023), patterns (Lin et al. 2023), detection (Xie et al. 2022), and predictions (Dong et al. 2022; Haque et al. 2022). The use of deep learning techniques and pretrained models in larger imagery areas has proven to be more robust, less laborious, and more accurate than manual inspections (Kaur et al. 2021; Chen et al. 2023). The unique landfall of the Shaheen Tropical Cyclone (STC), far north of the Arabian Peninsula, merits special consideration. Previous TC studies in Oman conducted land cover and land use techniques (Al-Hatrushi and Al-Alawi 2011), flood inundation analysis (Fritz et al. 2010; Al Ruheili et al. 2019; Banan-Dallalian et al. 2021), beach erosion assessment (Andreou et al. 2022), hydro(geo)logical assessment (Müller et al. 2020), statistical model analysis (Al-Manji et al. 2021), track data analysis (Al-Zadjali et al. 2021), and analytic hierarchy process (Mansour 2019).

Although numerous studies have been carried out globally to evaluate the effects of TCs using deep learning models, relatively few have been carried out in the Arabian Peninsula to fully assess the impact of TCs on the region's biodiversity, buildings, and water bodies. Moreover, none of the studies in Oman utilized the selected deep learning models with very high-resolution satellite imagery for the pre–impact and post–impact of the STC on a detailed level. Because we trained and applied deep learning models with GIS integration using extremely high-resolution satellite images (41 cm), this study is exceptional in its field applications. The selected deep learning libraries used in the study are proven to be fast and accurate in many objects' detection studies (Viraktamath et al. 2021; Lung and Wang 2023; Olorunshola et al. 2023), and impact assessment studies (Li et al. 2019). Therefore, this study aims to (1) train deep learning models using high-resolution satellite imagery and conduct an analysis of biodiversity due to STC landfall in Oman, and (2) pre–impact and post–impact assessment of STC on the biodiversity of the landfall areas. The study's findings offer invaluable insights that can empower landowners and government agencies to make informed decisions and strategically plan. By proactively addressing the post–cyclone impacts of climate change, these agencies can effectively safeguard Oman's urban areas and preserve their rich biodiversity. This foresight not only enhances resilience but also supports a sustainable future for the region. This study will help concerned authorities anticipate similar TCs at unexpected locations.

2 Materials and Methods

2.1 Study Area

The STC followed a rare path compared with other TCs in the Arabian Peninsula and made landfall on the northern coastline of the Sultanate of Oman on October 3, 2021 as shown in Fig. 2. Figure 3 shows the geographical location of the study area, consisting of the two most affected wilayats (Al–Khabourah and Al–Suwaiq) located in the North Al–Batinah Governorate of Oman, northwest of the Capital, Muscat. The study area experiences a hot and hyper-arid climate with an average temperature of 40 °C in summer and 20 °C in winter, and 100 mm average annual rainfall (Ali et al. 2021). The North Al–Batinah region is 1 m above mean sea level (Mansour et al. 2023) and covers the highest percentage of the total arable area (25.14%) in the Sultanate of Oman, with a total population of 833,766 people and a population density of 109 capita per Km^2 in the year 2022 (data.gov.om). During the STC period, 150, 214, 369, and 300 mm of rainfall were recorded in the wilayats of Musasnah, Saham, Al–Khabourah, and Al–Suwaiq, respectively, with an average for the four wilayats of 258 mm (MAFWR_OM 2021a).

2.2 Satellite Imagery Acquisition

This study utilized KOMPSAT-3 and GeoEye-1 satellite imagery with resolutions of 50 and 41 cm, respectively. The imagery was acquired before and after the impact of the STC for both wilayats in North Al–Batinah (Fig. 3). Cloud-free images were acquired before and after the impact of the STC on each wilayat to study its impact. The imagery acquired for the pre–impact analysis was obtained from the archives of the satellite platform in 2021. However, a new tasking from KOMPSAT-3 was requested for post–impact from the sensor platform to acquire the imagery of the area. Hence, post–impact imaging was performed between October 7 and 12, 2021, within 3–8 days after the impact. It is noteworthy to mention that the impacts of short-term flood receding or debris removal on the identification of damage can be a factor contributing to uncertainty of the aftermath analysis. However, an overall debris removal and cleaning activities for the STC, by the relief and shelter section, started on 8 October 2021 (Times of Oman 2021). The pre–impact and post–impact imagery went through Ortho-rectification, radiometric calibration, atmospheric correction, and geometric correction processes using ENVI 5.0 and ArcGIS

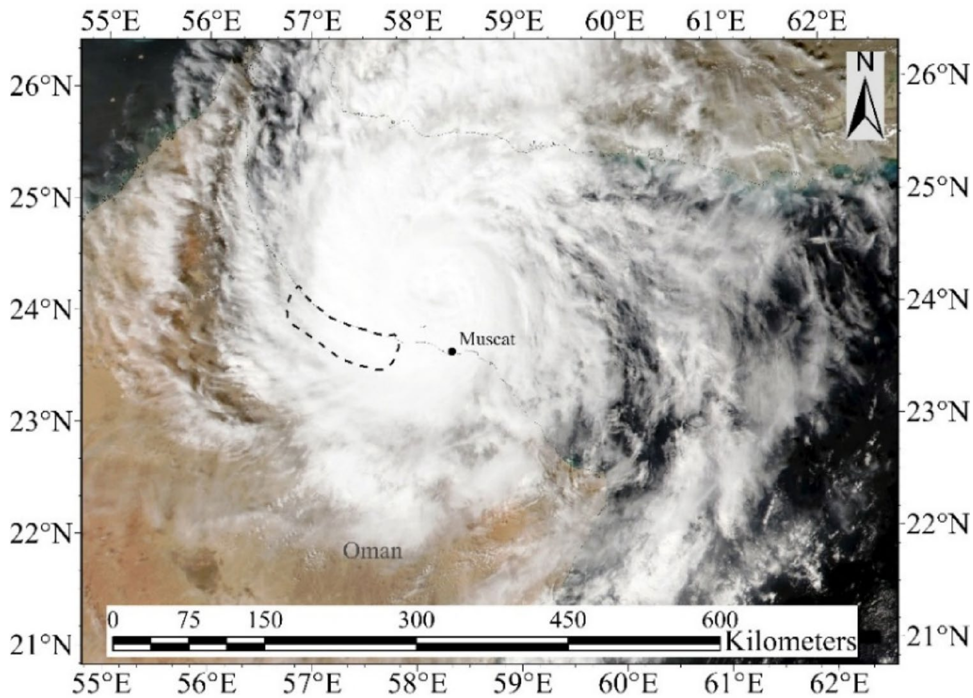

Fig. 2 True color imagery of the STC was captured on October 3, 2021, by the Moderate Resolution Imaging Spectroradiometer (MODIS) Terra satellite (NASA 2024), highlighting the study area with a dashed box

Pro, followed by image enhancement, geo-referencing, and mosaicking. More details about the satellite imagery and bands are provided in Table 1.

2.3 Methodology

Figure 4 illustrates the overall layout of the study conducted for the pre–impact and post–impact of STC over the study area. The following sections provide a detailed summary of these methods.

2.3.1 Artificial Intelligence in the Form of Multiple Deep Learning Techniques

Artificial intelligence in the form of Multiple Deep learning techniques was used in this study to detect and mask objects using a deep learning Framework installed in ArcGIS Pro (Version 3.2). The employed framework had all of the deep learning libraries (SSD, Mask R-CNN, and YOLOv3). Since there were no other updated YOLO versions available in the framework during our analysis for this study, YOLOv3 was used. The purpose of this framework was to facilitate geospatial analysis by generating layers of shapefiles for mapping, visualization, and additional evaluation. To the best of our knowledge, this study is among the first to use these deep learning libraries to evaluate the TC impact, as is also noted in the research gap section. The methodology used for implementing deep learning is illustrated in Fig. 5. The process began with downloading and installing the necessary deep learning algorithms to be activated within ArcGIS Pro. Subsequently, various objects were labeled to prepare the training data using the “Label Objects for Deep Learning” toolbox. Precise sampling of each object was performed using the ROI toolbox. An ROI boundary was drawn around each object in the sample imagery, after which the training samples were exported into multiple pixel sizes and model formats, as illustrated in Fig. 5. Training samples were exported in TIFF format with various sizes ranging from 64 to 400 pixels based on the objects presented in the study area. For this study, training samples were exported using the PASCAL Visual Object Classes, RCNN Mask, and KITTI metadata formats.

After preparing the data, the “Train Model for Deep Learning” tool was used to train each model using the training datasets and deep learning frameworks. First, all relevant training samples related to the objects of interest were imported to ensure that the model was trained specifically for the relevant objects. Second, the model type was selected based on object type and characteristics. To train the model for object detection and masking, different backbone models were used with different combinations of the model hyperparameters (Table 2).

First, the epochs were exported using the PASCAL format style and RCNN Mask format, employing three different patch dimensions: 256×256 pixels, 128×128 pixels, and 64×64 pixels. Each of these patch sizes included the location of the sampled object, along with the pixel number stored in a label text file located in the patch folder. After storing the epochs, they were individually used to train the model.

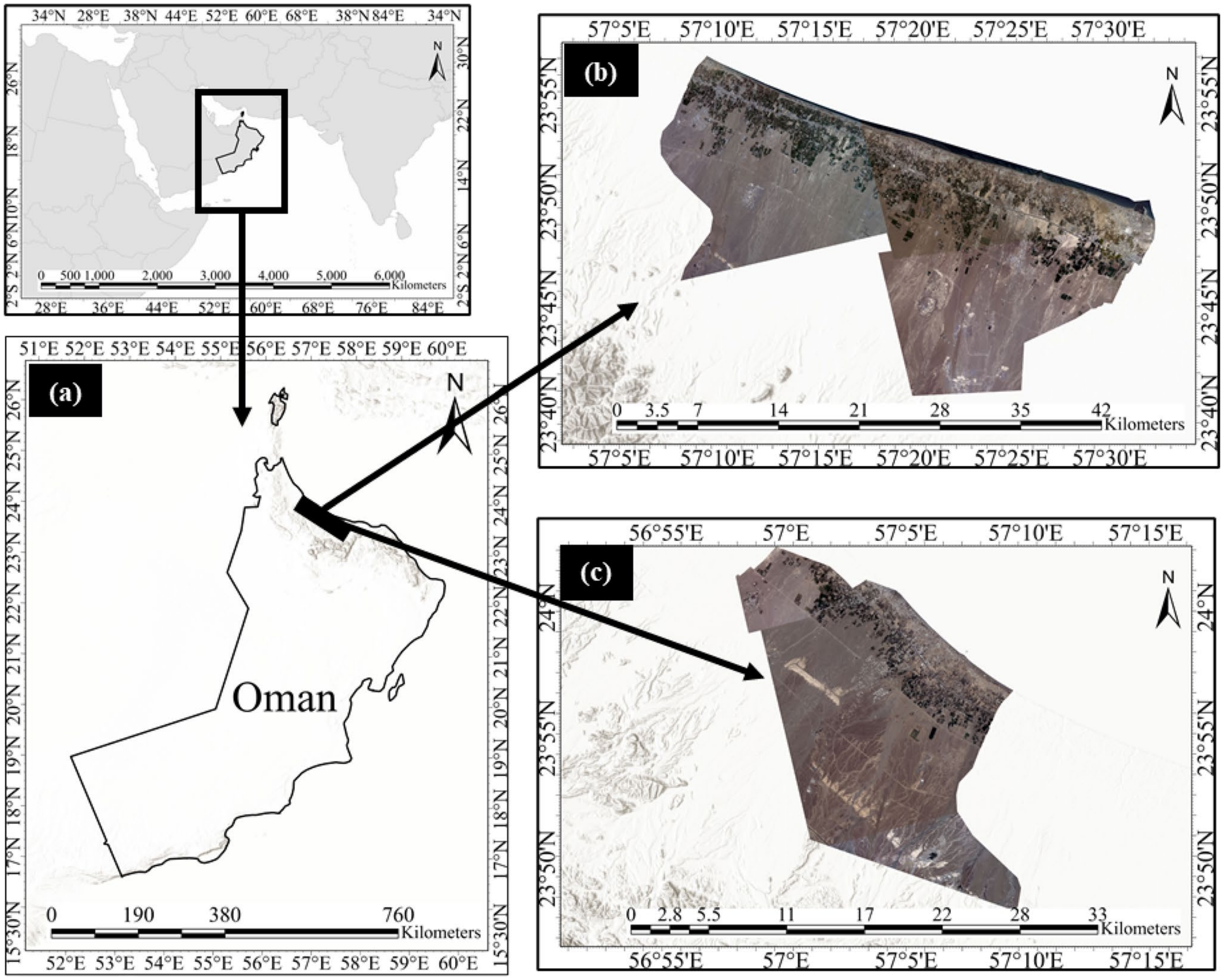

Fig. 3 Geographical location of (**a**) Oman and RGB overlay of the landfall areas of (**b**) Al–Suwaiq and (**c**) Al–Khabourah

Table 1 Specification of satellite imagery used in this study acquired between 11 May 2021, and 12 October 2021

Satellite Name	KOMPSAT-3	GeoEye-1
Spatial Resolution	0.5 m	0.41 m
Bands		
Blue	450–520 μm	450–510μm
Green	520–600 μm	520–580μm
Red	630–690 μm	655–690μm
Near-Infrared	760–900 μm	780–920μm

Each model was trained using different parameter selections for the various backbone models. This step was repeated until the losses and average precision could not be further improved. The results section presents the results of the selected deep learning model used in this study. The next section provides the basic principles of the model examined in this study.

2.3.1.1 Single Shot Detector According to Liu et al. (2016), Single Shot Detector (SSD) is a type of convolutional network (Fig. 6) that identifies objects in images and uses non-maximum suppression to help detect different object classes within fixed-size boxes. The SSD is structured into two integral blocks that work together to deliver powerful object-detection capabilities. The first block features a backbone model that proficiently extracts essential features using a pretrained image classification model. The second block, known as the SSD head, adds one or more convolutional layers to the backbone. It decisively outputs bounding boxes and accurately defines the spatial location of each detected object. More details regarding SSD can be found in Liu et al. (2015, 2016).

2.3.1.2 Mask R–CNN Mask R–CNN (Fig. 7) is a straightforward, adaptable, and universal framework utilized for

Fig. 4 Illustration of the study approach

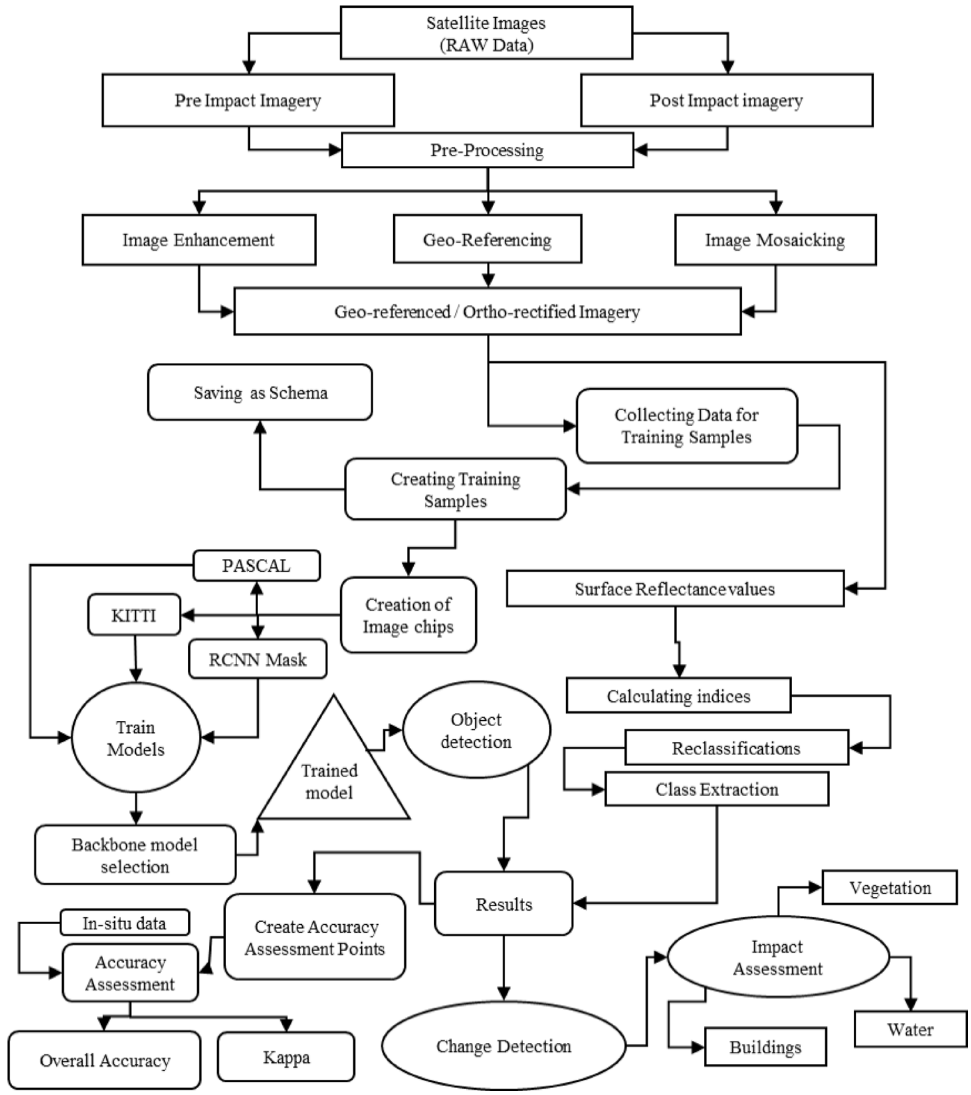

object segmentation, which builds upon Faster R–CNN by incorporating an additional branch that identifies and predicts a mask concurrently with the existing branch for bounding box recognition (Banan-Dallalian et al. 2021).

2.3.1.3 YOLOv3 (You only Look once v3) You Only Look Once version 3 (YOLOv3) is one of the most widely used object detection models based on deep learning; it employs the K–means clustering method to estimate the dimensions and size of objects, as well as to define their bounding boxes using ResNet family backbone models (Zhao and Li 2020). According to Redmon and Farhadi (2018), YOLOv3 builds upon advancements in YOLOv2, enhancing its capabilities. It transitions from an earlier DarkNet–19 to a more robust deep architecture known as DarkNet–53, which features 53 convolutional layers. This deeper structure (Fig. 8) allows YOLOv3 to effectively improve object detection performance.

2.3.1.4 Water Bodies To train the water detection model, we used the pixels of water bodies from the satellite imagery that is used in the study as later showed in the results section (a) that there was no water stored in the dam before the STC landfall. Same trend was also observed in other parts of study area. This scenario led to low number of water bodies allocated for the training the model which could lead the model to overfitting and further, unrealistic results. Hence, the Normalized Difference Water Index (NDWI) was used in this study. The NDWI is a satellite imaging tool that highlights open water features, allowing them to stand out against soil and vegetation. NDWI was developed to detect water in flooded areas during extreme weather events, thereby enhancing the presence of open water fea-

Fig. 5 Layout of the methodology used to train the model

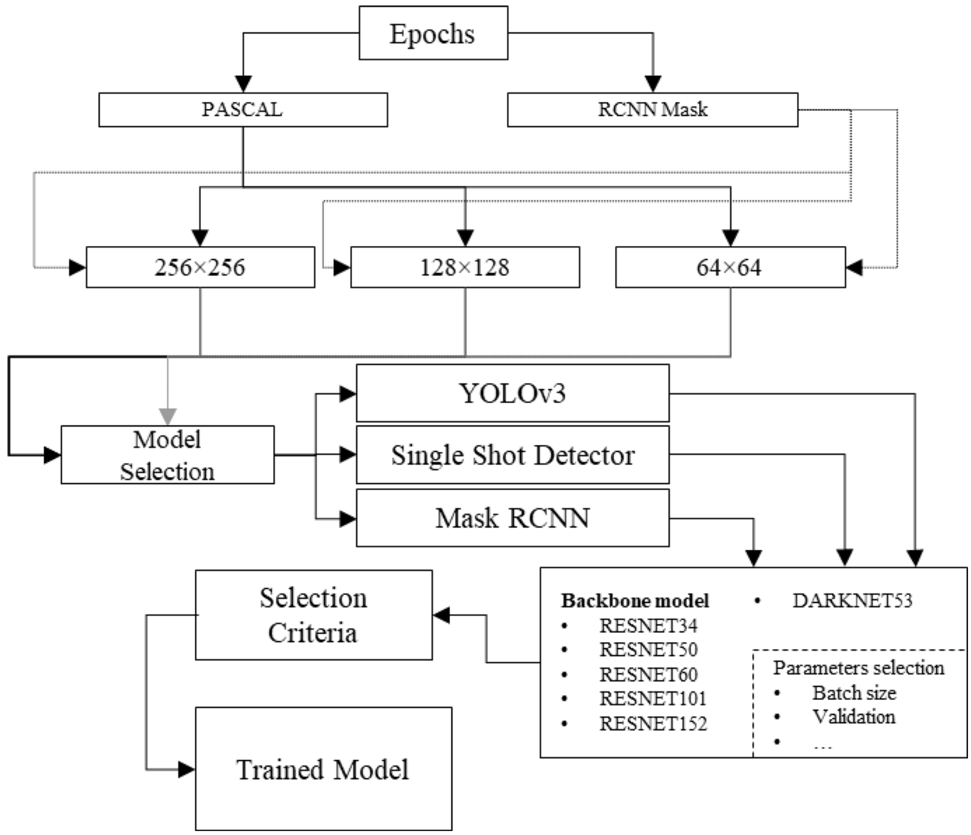

Table 2 Details of hyperparameters used for training the deep learning models

Model	Epochs	Batch	Learning Rate	Validation
Mask R–CNN	20–40	4–64	0.00001–0.0007	10%
YOLOv3	20–100	64–120	0.00004–0.003	10%
SSD	20–60	16–120	0.0002–0.0017	10%

tures in remotely sensed digital imagery. NDWI uses green and near-infrared bands to detect subtle changes in the water content. NDWI was first proposed in 1996 and is less sensitive to atmospheric effects than NDVI (Gao 1996). NDWI values ranged from −1 to 1, and the positive values corresponded to water only and have been used in many studies to detect water bodies and delineate the impact of TCs on existing and new water bodies (Prakash et al. 2023; Hungwe et al. 2024; Mishra et al. 2024). To estimate NDWI, the reflectance values of the bands were converted to NDWI values using raster calculation in ArcGIS Pro using Eq. 1.

$$NDWI = {(\gamma_G - \gamma_{NIR})} \Big/ {(\gamma_G + \gamma_{NIR})} \tag{1}$$

Fig. 6 Architecture of the Single Shot Detector (SSD) model

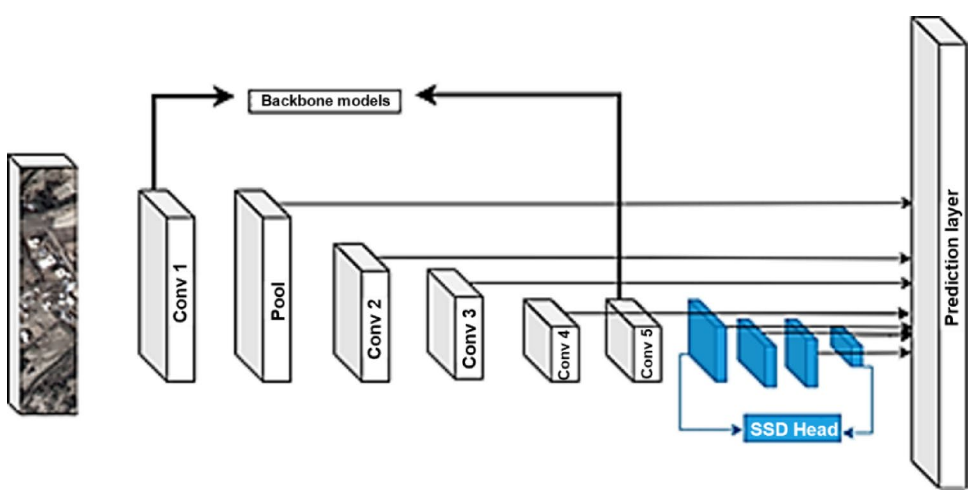

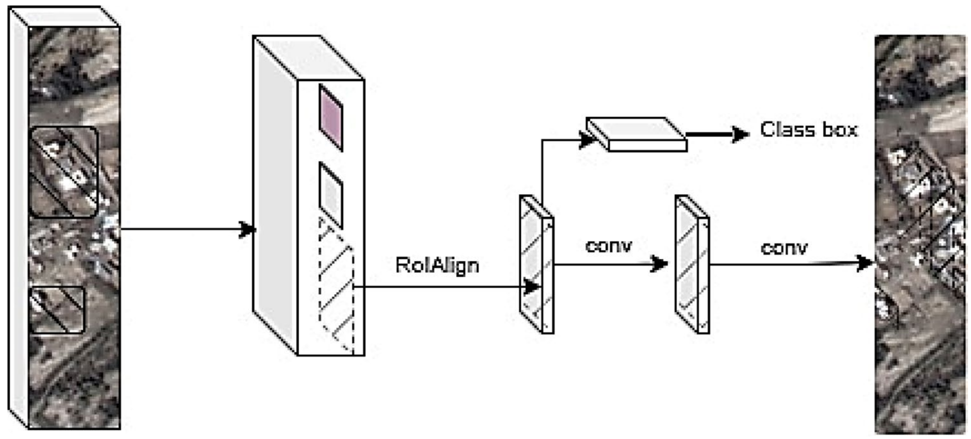

Fig. 7 Graphical architecture of the Mask R–CNN model (He et al. 2020)

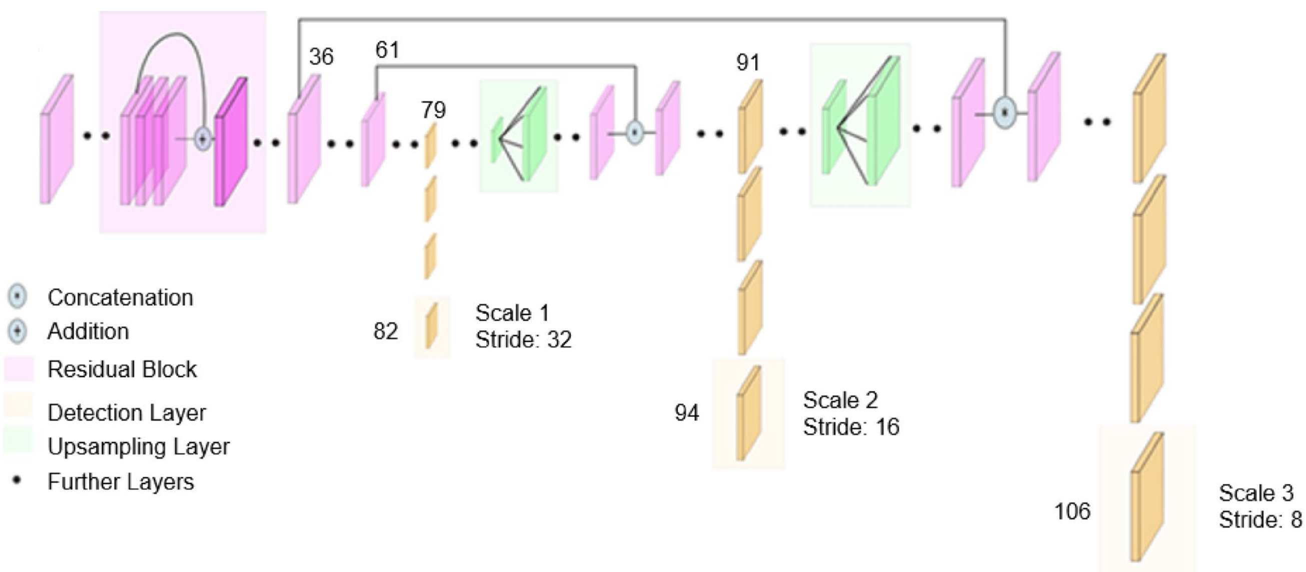

Fig. 8 Architecture of the YOLOv3 model (Kathuria 2018)

Where NDWI is Normalized Difference Water Index, while γ_{NIR} and γ_G are near-infrared and green bands of satellite imagery, respectively.

NDWI maps were constructed for pre–impact and post–impact. NDWI maps were constructed and reclassified according to the water body values. The locations of the existing water bodies were identified using the pre–impact assessment, and these locations were subsequently utilized to investigate the physical impacts of the STC on the water of these bodies.

2.3.1.5 Vegetation TCs have severe effects on vegetation, loss of agricultural development, and the economy (Feehan et al. 2024). First, we used the trained deep-learning models to detect vegetation in the study area by creating a 2D detection box that was saved as shapefiles. These shape files were used as vegetation masks to extract only the vegetation areas. Once vegetation was detected, the next step was to categorize these detections based on their Normalized Difference Vegetation Index (NDVI) values, as many studies have used vegetation indices to assess the impact of TCs on vegetation (Charrua et al. 2021; Kai et al. 2021; Shamsuzzoha et al. 2021). Moreover, NDVI has proven its significance in vegetation categorization and assessment (Al-Mulla et al. 2022; Al-Kindi et al. 2023). For the vegetation impact analysis, the pre–impact and post–impact vegetation categories were calculated using Eq. 2 for STC.

$$NDVI = {}^{(\gamma_{NIR} - \gamma_R)}\Big/{}_{(\gamma_{NIR} + \gamma_R)} \tag{2}$$

Where, NDVI is Normalized Difference Vegetation Index, while γ_{NIR} and γ_R are the near-infrared and red bands of satellite imagery, respectively.

NDVI maps were constructed for the pre–impact and post–impact. NDVI maps were created in the detected vegetation categories and classified according to the values representing the vegetation type (dense, sparse, and shrub/grassland). Before the STC made landfall in the study area, the coordinates of the previously available vegetation parcels were collected using the Google Earth Pro archives. These samples were also used as accuracy points to detect changes in vegetation.

2.3.1.6 Building Areas consisting of buildings near the coasts are most affected by TCs due to high wind speed, waves, debris, and high moisture in the air (Hong et al. 2025). We trained and used deep learning models to classify buildings from other objects/features in the satellite imagery. Figure 5 shows the layout of the deep learning model used to detect and map the buildings. The building extraction was also validated against in situ data collected from Google archive imagery using the Google Earth Engine. This method was repeated for post–impact detection, and a change detection map was generated, highlighting the affected areas of the buildings.

2.3.1.7 Digital Elevation Maps A digital elevation map (DEM) presents an overall scenario of a region, highlighting the area's height and assisting in determining its vulnerability to potential cyclone/disaster impacts. The study of the elevation of an area is also crucial to determine whether the area is exposed to a possible storm surge. We used an innovative technique to draw elevation maps of the study area using the elevation profiles from Google Earth Pro. The elevation data were recorded from Google Earth Pro with the corresponding coordinates, imported, and then interpolated using inverse distance weighted (IDW) interpolation in ArcGIS Pro (version 3.2). These elevation maps have proven to be more accurate at the inquiry stage for primary road, drainage, and watershed boundary delineation (Anis-Athirah et al. 2021; Rochmadi 2023).

2.3.1.8 Terrain Ruggedness Index (R) The Terrain Ruggedness Index (R) highlights the amount of elevation difference between adjacent cells of the DEM, providing spatial variability insights into the surface area (Trevisani et al. 2023). R is used to express the amount of elevation difference between adjacent cells to a point and has been widely used in many studies (Kaspi and Kuleshov 2023; Okolie et al. 2023). First, the values of the neighboring pixels were subtracted from those of the central pixel (under calculation). The differences were then squared, added to each other later, and squared again. The methodology used in this study to estimate R is described in detail in Riley et al. (1999). Equation 3 shows the process in its simplest form:

$$R = \left(\sum (E_c - E_i)^2\right)^2 \tag{3}$$

Where R is the Terrain Ruggedness Index, while E_c is the value of the pixel being calculated, and E_i is the value of the surrounding pixel, where i values range from 1 to 8.

2.3.1.9 Hot Spot/Cold Spot Analysis Hotspot analysis is a helpful tool for recognizing spatial clusters of both high and low values. This tool has helped many studies to highlight the TCs impact in different areas around the globe (Hassan et al. 2020; Zhou et al. 2021; Luo and Wu 2022). This tool works by examining each feature within the context of neighboring features. A feature with a high value is interesting but may not be a statistically significant hotspot. The hotspot technique identifies statistically significant spatial clusters of highly flooded areas as hot spots and non-flooded areas as cold spots. This results in an output feature class with z-score, p-value, and confidence level bin (G_i^*) for each feature in the input feature class. Based on the G_i^* (Eq. 4) values, statistically significant hot and cold spots were identified, corrected for multiple testing and spatial dependence using the False Discovery Rate (FDR) correction method. More details regarding hotspot analysis can be found in ESRI (2023a, b).

$$G_i^* = \frac{\sum_{j=1}^{n} w_{i,j} x_j - \overline{X} \sum_{j=1}^{n} w_{i,j}}{S\sqrt{\frac{\left[n \sum_{j=1}^{n} w_{i,j}^2 - \left(\sum_{j=1}^{n} w_{i,j}\right)^2\right]}{n-1}}} \tag{4}$$

Here $G_i^*$is confidence level bin for each feature (i) where x_j is the attribute value for feature j, $w_{i,j}$ is the spatial weight between features i and j, and n is the total number of features. The values of $\overline{X}$and S are calculated using Eqs. 5 and 6.

$$\overline{X} = \frac{\sum_{j=1}^{n} x_j}{n} \tag{5}$$

$$S = \sqrt{\frac{\sum_{j=1}^{n} x_j^2}{n} - \left(\overline{X}\right)^2} \tag{6}$$

2.4 Accuracy Assessments

The accuracy assessment analyses were conducted in two phases using random distribution techniques. In the first phase, more than 150 locations were randomly selected with different land cover types (feature classes) in pre–impact and post–impact and recorded with a GPS device (Garmin Montana 700). These locations were then used as ground truthing points by adding the feature class from the results of the current study using satellite imagery and Google Earth Pro RGB imagery archive. The second phase used a support vector machine learning algorithm procedure, which involved performing a confusion matrix analysis to measure the accuracy of the impact assessment. The criteria used in the accuracy assessment of this study were as follows:

$$Precision = \frac{TP}{(TP + FP)} \tag{7}$$

$$Recall = \frac{TP}{(TP + FN)} \tag{8}$$

$$F1 - Score = \frac{2 \times Precision \times Recall}{Precison + Recall} \tag{9}$$

$$Macro - F1 = \frac{\sum F1 - Score}{N} \tag{10}$$

$$Weighted - F1 = weighted_{averaged} of\ F1\ Scores \tag{11}$$

$$Misclassification\ Rate = \frac{Incoreeect\ Predictions}{Total\ Predictions} \tag{12}$$

Where TP, FP, and FN are True positives, false positives, and false negatives, respectively. While N is the total number of samples. On the other hand, $F1 - Score$ is the harmonic mean of Precision and Recall, $Macro - F1$ is the average of $F1 - Score$ of each class, and $Misclassification\ Rate$ is the proportion of incorrectly predicted instances.

3 Results and Discussion

3.1 Deep Learning Models

Figure 9 illustrates the average precision score of the trained deep learning model used to detect and map buildings and vegetation in the study area. Various combinations of model parameters were explored along with different backbone models to achieve the highest precision score for each category. This optimization process was crucial for enhancing the model's ability to accurately classify and differentiate between buildings and vegetation in satellite imagery. However, the models for the buildings and vegetation were successfully trained, as shown in Fig. 9. For the water bodies, NDWI was used to delineate water bodies in the study area.

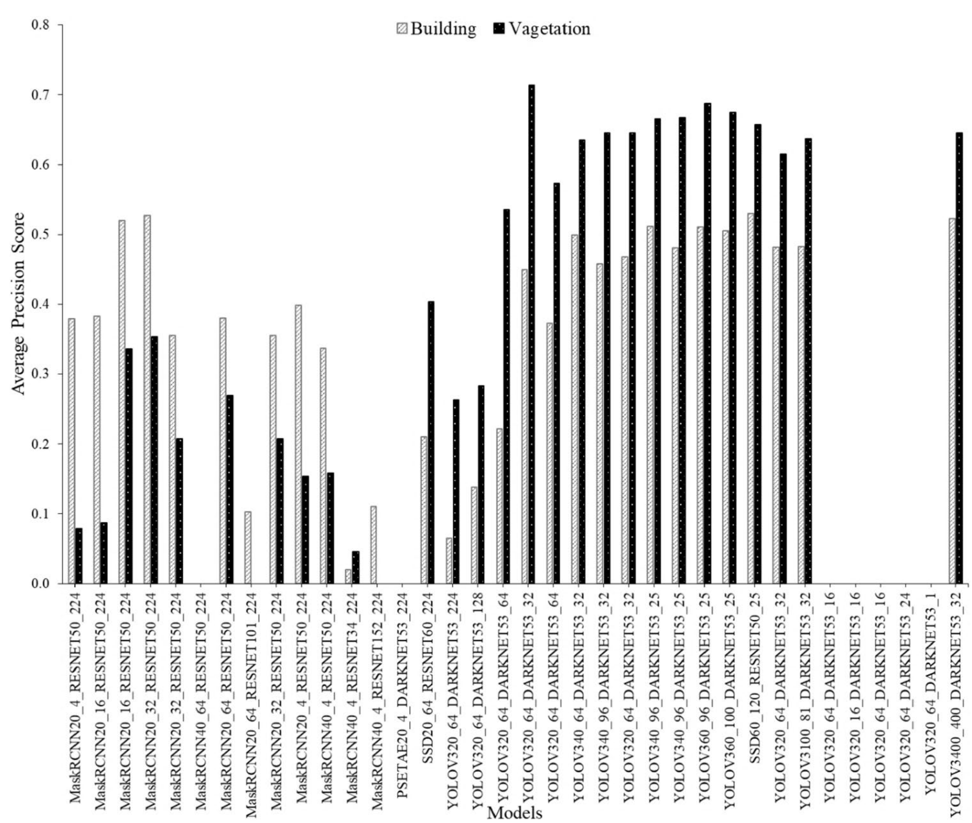

Fig. 9 Variation in average precision score of deep learning models trained for detecting and mapping buildings and vegetation

In this study, approximately 40 different combinations of backbone models, each with varying parameters and batch sizes, were used. Figure 9 illustrates the results of these models, showing the impact of different epoch quantities, models, backbone types, chip sizes, and batch sizes on the overall precision score achieved. The trained models with the highest average precision scores were selected to detect and map objects in the satellite imagery.

3.2 Impact on Water Bodies

On October 1, 2021, remnants of the Gulab cyclone (formed in the Bay of Bengal in September) coalesced to create STC northeast of the Arabian Sea. Figure 10 shows the track record of the STC for every three hours and the cumulative rain between October 2 and 3 (before the STC landfall). The rainfall data showed that the wilayat of Bousher (no. 5 in Fig. 10) received the highest amount of rainfall (189 mm) between October 2 and 3, while the lowest rainfall was recorded in the wilayats of Ibri (no. 54 in Fig. 10), Sur (no. 28 in Fig. 10), and Saham (no. 23 in Fig. 10) with 1 mm, 2 mm, and 3 mm, respectively. In contrast, Al–Suwaiq (no. 58 in Fig. 10), Al–Musanah (no. 10 in Fig. 10), and Al–Khabourah (no. 29 in Fig. 10) received 130, 72, and 9 mm of rainfall, respectively, during the same period.

Figure 11 shows the rainfall recorded between October 3 and October 4, as STC made landfall on October 3, 2021, around 7 PM local time (Deutsche 2021). The rainfall data showed that the maximum rainfall was recorded in Al–Khabourah (no. 29 in Fig. 11), with 360 mm in the period of STC landfall (between October 3 and October 4). The dam storage data collected on 4 October by the Ministry of Agriculture, Fisheries and Water Resources, Oman, shows that the dam at the study area was at its full capacity of 3.7 million m^3 and started overflowing toward the head of Wadi Al–Hawasnah Lagoon in Al–Khabourah (MAFWR_OM 2021b).

Figure 12 shows the cumulative rainfall between October 2 and October 4 in the study area. The findings indicated that during the STC, Al–Khabourah (no. 29 in Fig. 12) experienced the maximum cumulative rainfall (369 mm), followed by Al–Suwaiq (no. 58 in Fig. 12) at 300 mm, and Saham (no. 23 in Fig. 12) at 214 mm. In contrast, As-Seeb (no. 60 in Fig. 12) recorded 222 mm, Barka (no. 17 in

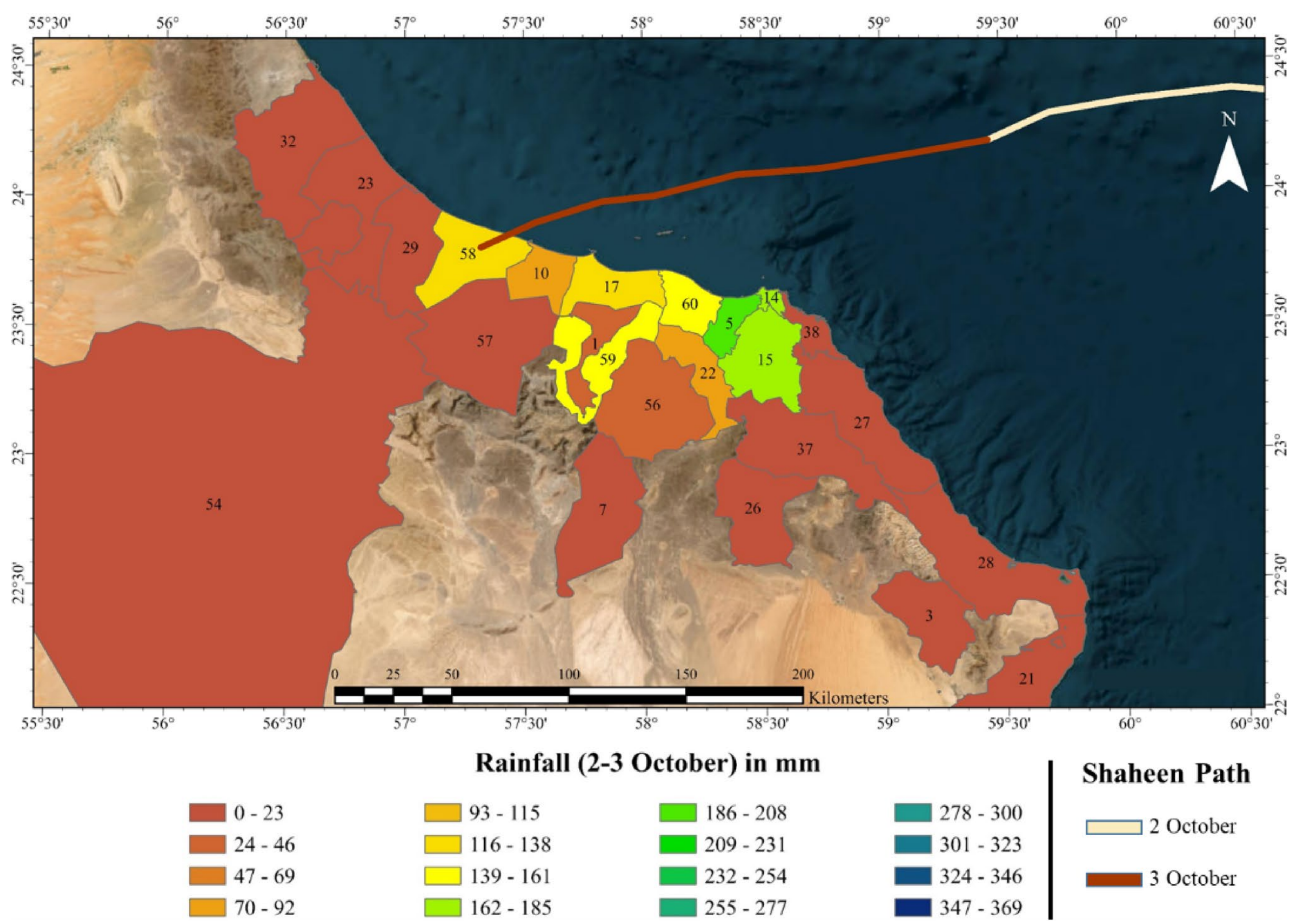

Fig. 10 Spatial distribution of the rainfall recorded in the study area (before the landfall) between 2–3 October 2021 and tracks of the STC

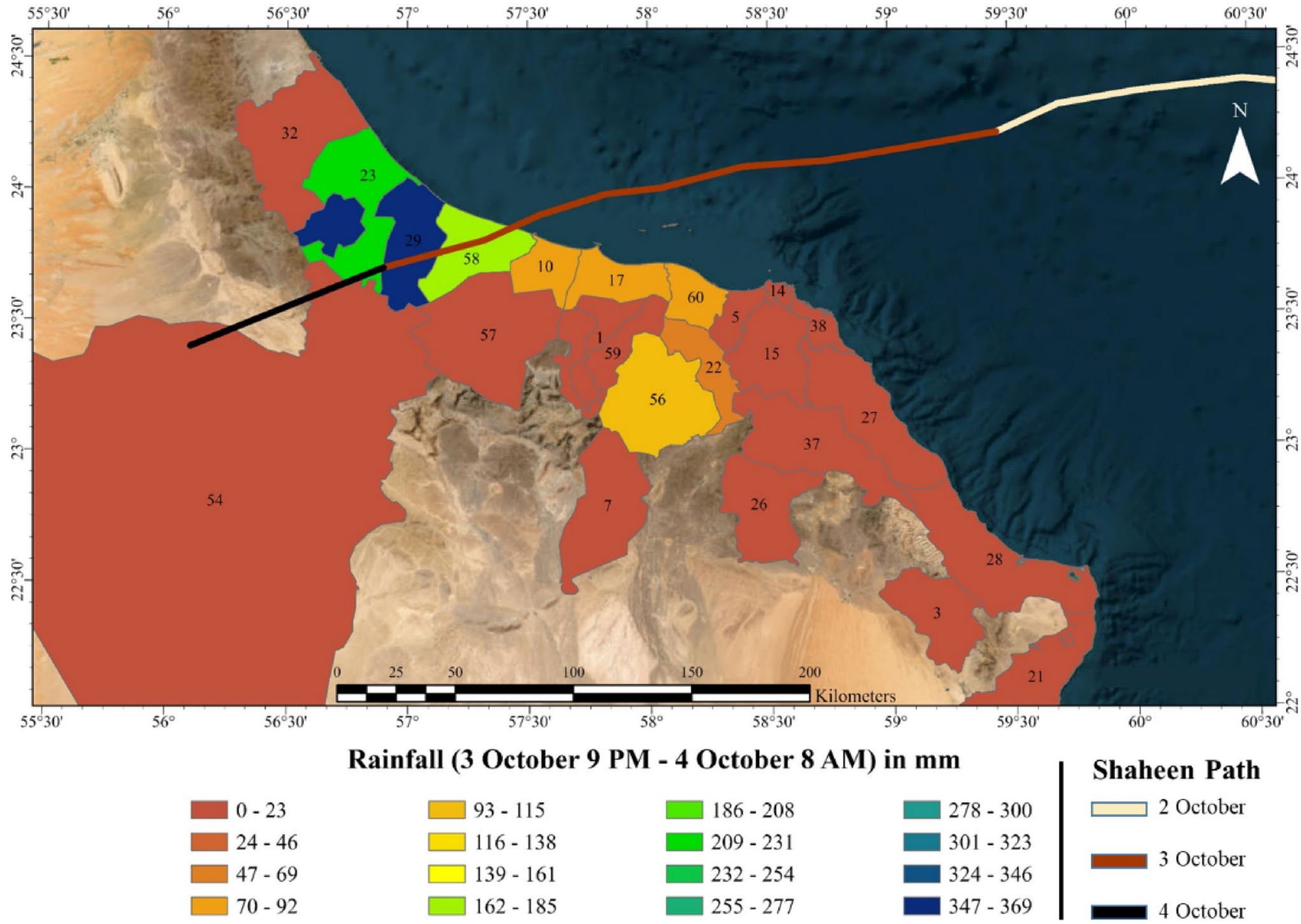

Fig. 11 Spatial distribution of the rainfall recorded in the study area (during the landfall) between 3 and 4 October 2021 with overall tracks of the STC

Fig. 12) received 203 mm, and Bousher (no. 5 in Fig. 12) received 202 mm of rainfall.

On the other hand, satellite imagery was also used to extract water features from the study area, and a change detection analysis was performed to record the changes in the water bodies. Before conducting the water analysis, we classified the water bodies into two categories: shallow water and water pools. Shallow water included water with less than a meter depth, while water pools included larger amounts of water deeper than the shallow water that formed in cities or wadies, especially in places with deep slopes.

Because some water bodies existed before the STC impact, the change detection analysis considered the water coverage that existed before and after the impact. Figure 13 shows the spatial variation in the water bodies before and after the impact of STC.

Figure 13 (a) shows the impact of STC on the wilayat of Al–Khabourah. Figure 13 (a1) shows the spatial distribution of water detected in Wadi Al–Hawasnah and Wadi Bani Omar, and Fig. 13 (a2) shows the presence of water in Wadi Al–Hawasnah and Wadi Bani Omar Dam. Prior to the impact, results showed that 0.09 ha of shallow water and 0.07 ha of pool water were found. These water areas increased to 335.3 ha and 161.6 ha, respectively, following landfall of the STC (Fig. 13b).

The spatial distribution of water found in the Al–Suwaiq wilayat is shown in Fig. 13(c). Figure 13 (c1) shows the water bodies detection in the urban areas located near the coast, whereas Fig. 13 (c2) shows the water detected in the wadi located in the wilayat. Before the STC impact, change detection analysis revealed 140.3 ha of shallow water and 0.35 ha of water pools. Following the STC landfall, these water areas expanded to 232.1 ha for shallow water and 89.42 ha for Water pools, respectively (Fig. 13d).

3.3 Impact on Vegetation

The STC landfall impacted vegetation in both wilayats. The vegetation maps constructed from high-resolution satellite imagery were classified into four vegetation levels: non-vegetation, shrubs and grasslands, sparse vegetation, and dense vegetation. The non-vegetation area category

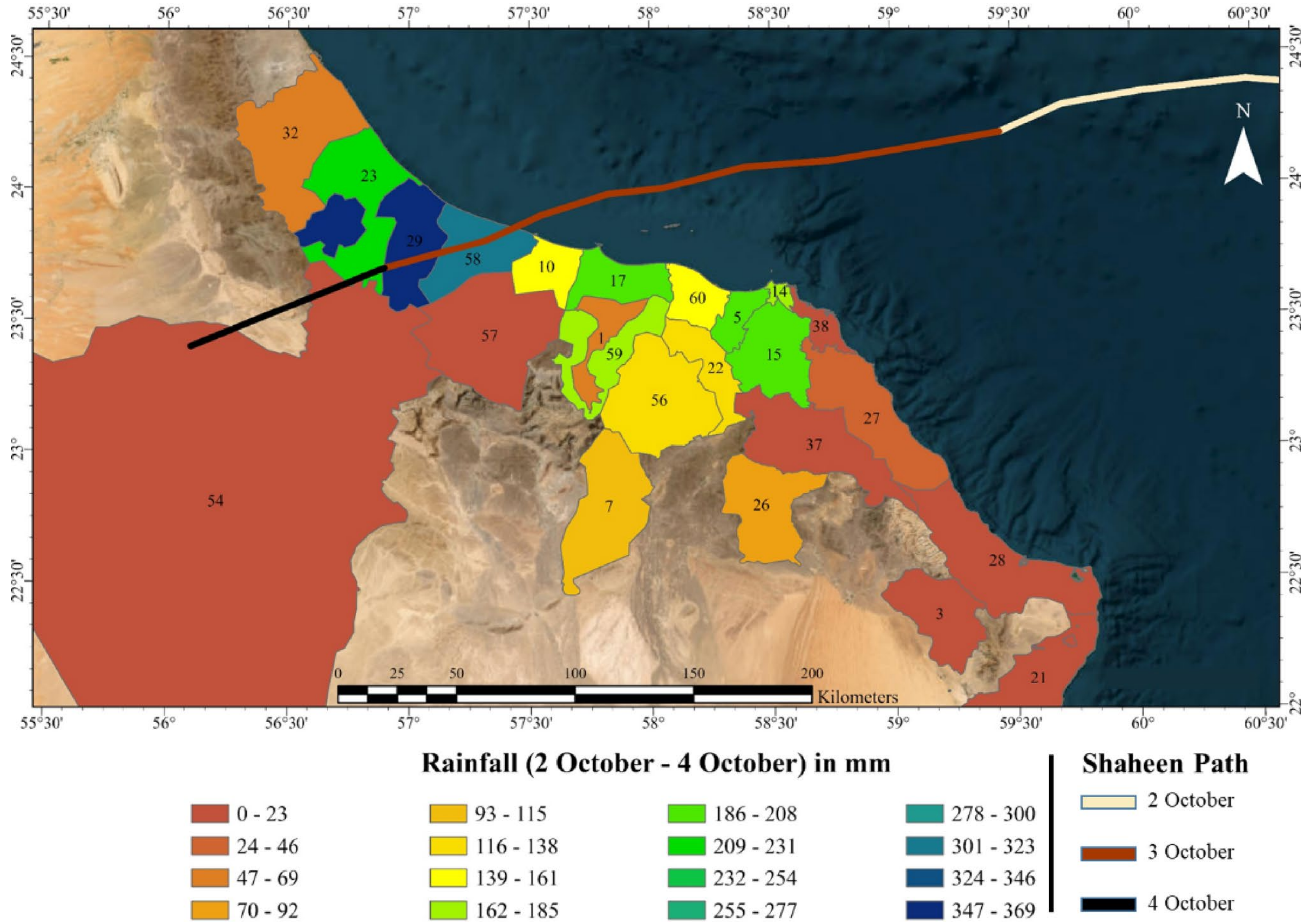

Fig. 12 Spatial distribution of the cumulative rainfall recorded in the study area between 2 October and 4 October 2021 with a complete track of the STC

included a mixed class of soils and other objects. Shrubs and grasslands cover individual trees and grasslands, while sparse vegetation covers freshly cut Rhodes grass fields and other crops.

The results from this study showed a 9.8% loss (274 ha) of the total vegetation in the wilayat of Al–Khabourah. Figure 14(a) shows the impact of STC and the damaged area with the loss of vegetation in wilayat Al–Khabourah. The change detection analysis (Fig. 14b) showed that 1.9% (35 ha) of shrubs and grasslands were destroyed, while 18.9% (153.16 ha) of sparse vegetation was completely wiped out. A severe effect was observed on dense vegetation, with a loss of 51.3% (85.8 ha). The major affected area in Al–Khabourah was the downstream area of the Wadi Al–Hawasnah and Wadi Bani Omar Dam. This dam was constructed 8.5 km away from the coastline in the Wadi Al–Hawasnah in 1995, and the drainage area of this dam opens to the Wadi Al–Hawasnah lagoon, which was surrounded by the date palm farms (Al-Hatrushi 2013).

Vegetation has been severely damaged in the confluence point where Wadi Hawasnah and Wadi Bani Omar form a lagoon near the coast. Due to the wadi flow and intense rainfall, most of the vegetation in the farm was completely wiped out. Moreover, it was observed that construction adjacent to the lagoon was completely wiped out by erosion and water surge in the wadi. It is also observed that the farm located near the wadi passage was severely damaged.

The impact of the STC on vegetation in the Al–Suwaiq layout is shown in Fig. 15(a). The analysis of vegetation maps showed that Al–Suwaiq was the most affected wilayat among the other wilayats. Figure 15(a) shows that STC affected all vegetation types, especially near the coastline, where most vegetation was completely wiped out. The impact was also visible in the south of the Al–Batinah highway because the flowing wadis/floods eroded soil/boulders and debris, which damages roads, infrastructure, and vegetation. Vegetation analysis in Fig. 15(b) showed a 5622 ha (13.15%) increase in non-vegetative areas. Change detection on vegetation maps showed that 3160 ha (55.5%) of shrubs and grasslands, 1714 ha (67.2%) of dense vegetation, and 610 ha (16.6%) of sparse vegetation were completely damaged after the impact. The change detection analysis in

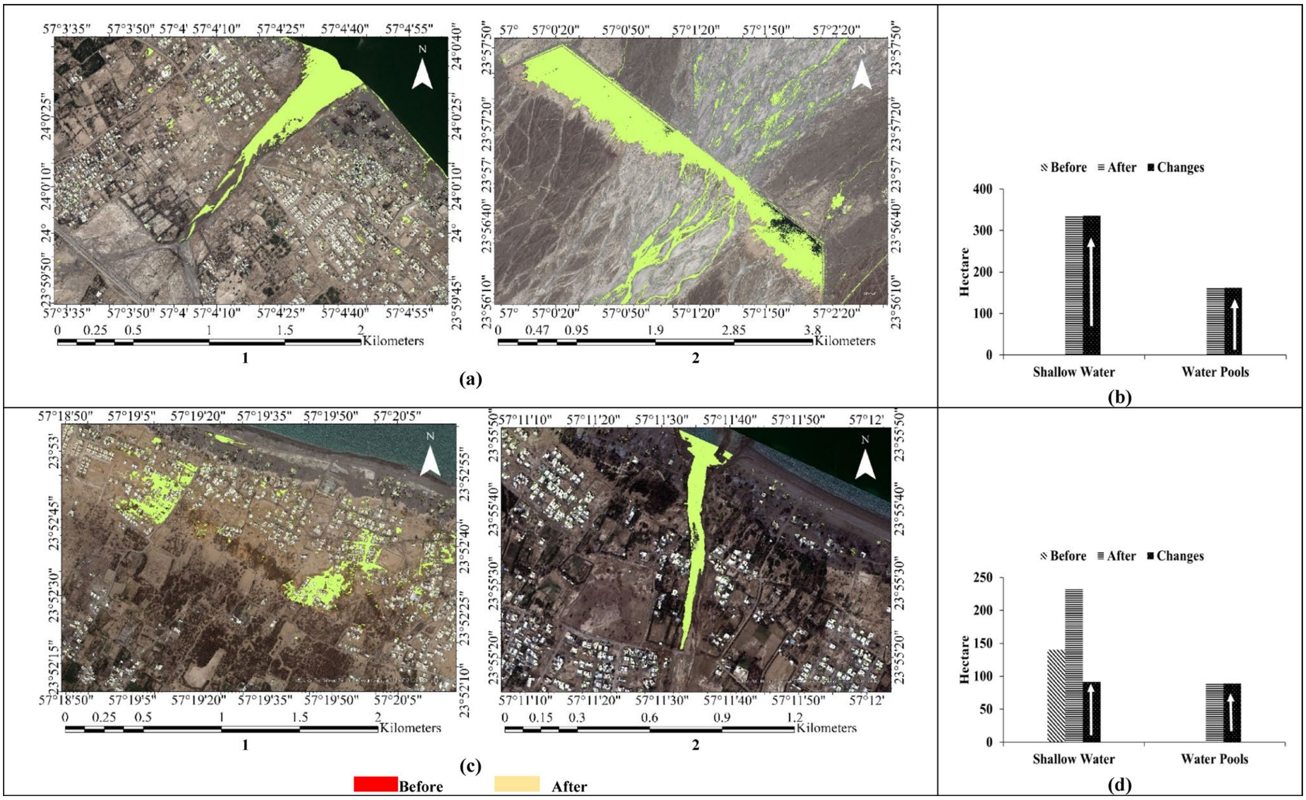

Fig. 13 Pre–impact (red) and post–impact (yellow) water bodies in (**a**) Al–Khabourah and (**c**) Al–Suwaiq, while, Pre–impact (column with inclined lines), Post–impact (column with horizontal lines), and cumulative area changes (black column) in water bodies in (**b**) Al–Khabourah, and (**d**) Al–Suwaiq

Al–Suwaiq (Fig. 15b) revealed that STC destroyed 5484 ha (from 11926 ha to 6442 ha) of all vegetation during the study period.

Figure 16 shows the overall impact of the STC on vegetation in the study area. It was observed that the overall vegetation in the study area decreased after the STC impact. The results indicated that 5317.3 ha (3.5% loss) of all types of vegetation were damaged after the STC impact. The study resulted in 1730.1 ha of dense vegetation in the study area being damaged, which was 57.42% of the total dense vegetation before the STC impact. On the other hand, the same trend was observed in sparse vegetation, which reduced from 6588.8 ha to 5045.73 ha (23.42% loss). STC also impacted the shrubs and grasslands, which reduced from 9268.8 ha to 7224.6 ha (22.1% loss).

3.4 Impact on Buildings

The STC has also impacted buildings and urban areas as STC made landfall in the area. The rainwater flowing at high speed from the mountains in the wadis brought mud, debris, and large boulders that destroyed the property in the line of flow. According to the Civil Aviation Authority (2021), high wind speeds and heavy rainfall affected the Al–Kahbourah. AlRuheili (2022) investigated the impact of STC in Al–Khabourah, claiming an average erosion rate of 16.33 m/year in Al–Khabourah due to extreme events over short periods. Such effects were also observed in the STC impact assessment, as many houses, especially in Al–Khabourah, were partially destroyed (Fig. 17). The analysis resulted in STC affecting approximately 42.73 ha (32%) of the structures in Al–Khabourah. The impact caused significant damage along the beach, with 6.4 ha (67.5%) of the buildings being destroyed. Some of these structures were temporarily constructed by fishermen, usually made of date palm leaf blinds to keep boats and other belongings safe under shade. Structures (as shown in Fig. 17) built near the wadi and coastal regions were primarily destroyed because floodwater entered the residences and caused damage by partially covering them with mud and damaging the surroundings and boundary walls, which coincided with what was reported by locals (Observer 2021). Moreover, a survey conducted by Joseph et al. (2023) was conducted in the STC-impacted areas and found that 79% of the surveyed participants reported damages to their households, but their study underrepresented the area outside the direct impact.

Our study was able to provide a more detailed impact assessment of the STC in the area compared to other studies

Fig. 14 Change detection map of vegetation showing the destroyed in red colour, existing vegetation in Yellow, and Wadi paths in Blue line (**a**) and Changes in vegetation classes in the wilayat of Al–Khabourah (**b**)

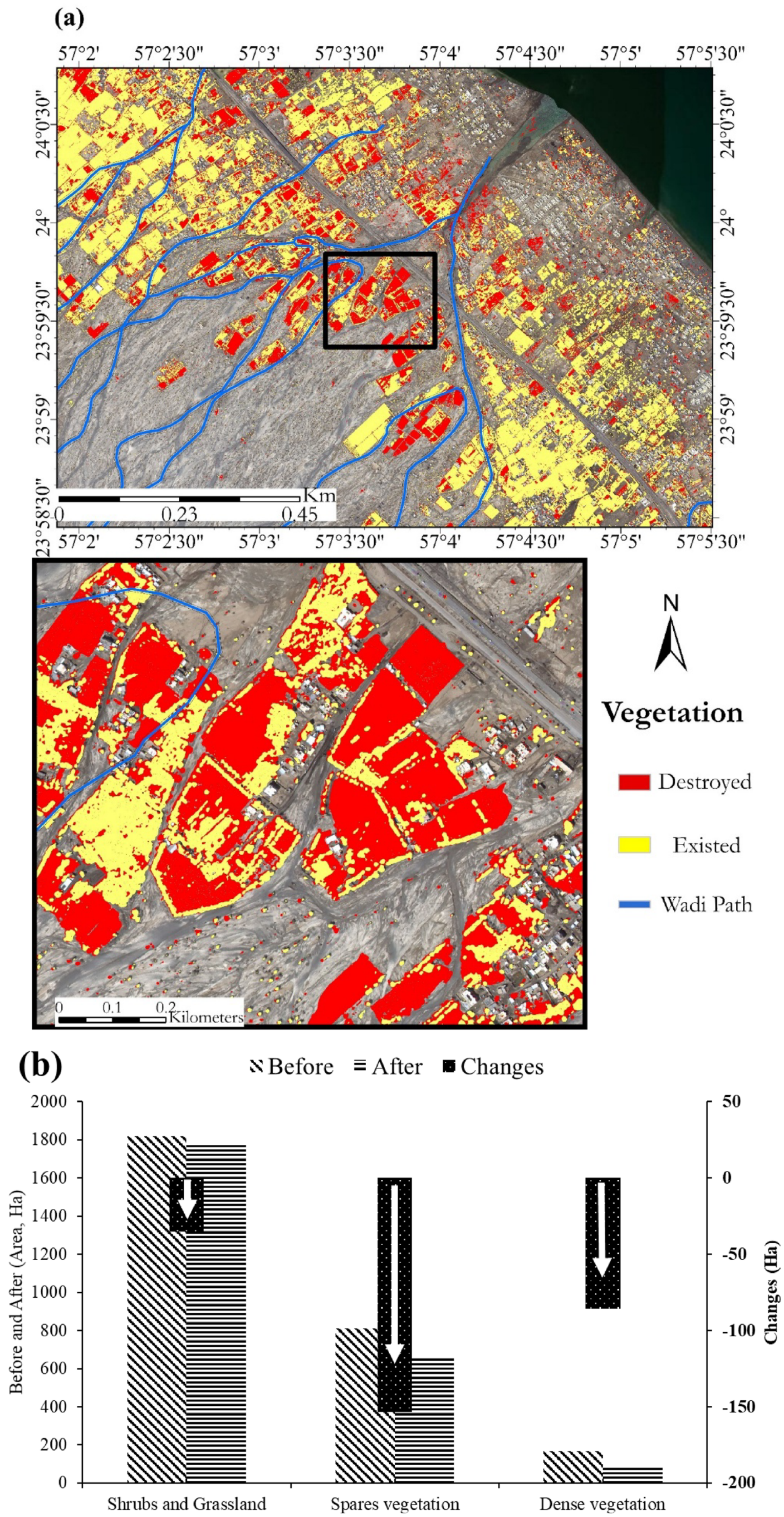

Fig. 15 Change detection map of vegetation showing the destroyed vegetation (Red), existing vegetation (Yellow), and Wadi paths in (Blue) (**a**) and Changes in vegetation classes in the wilayat of Al–Suwaiq (**b**)

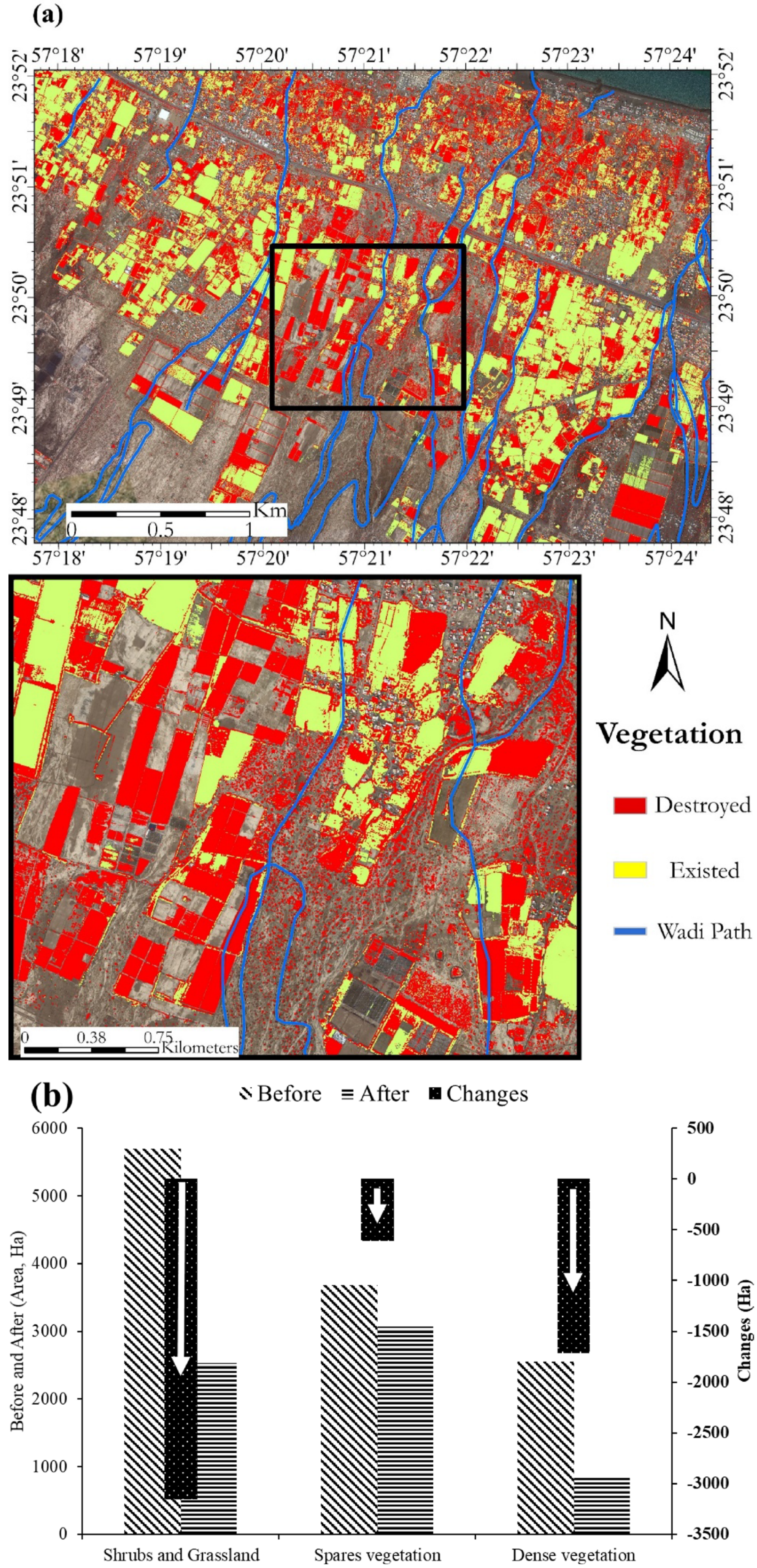

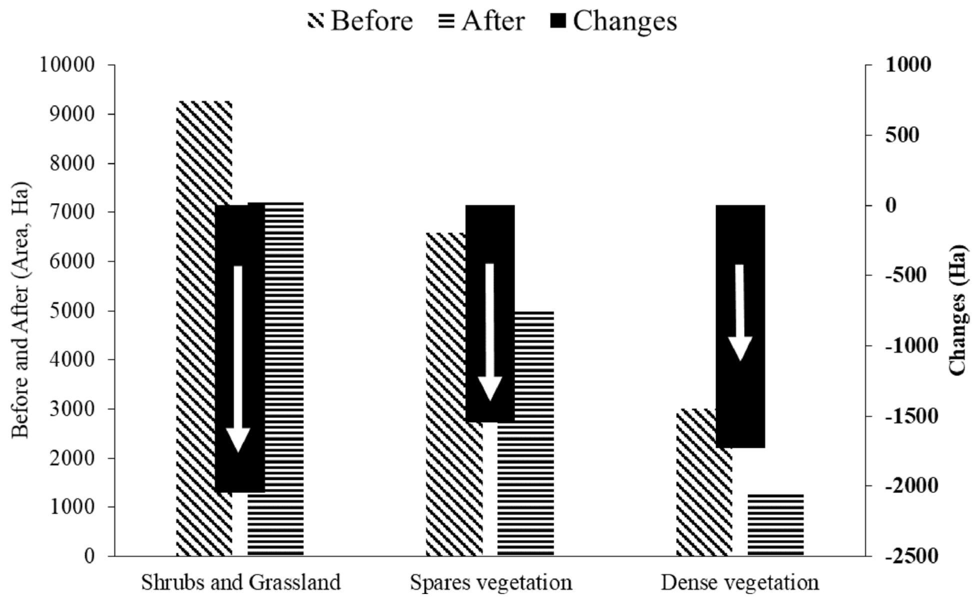

Fig. 16 Overall changes in the vegetation classes in the study area following the STC impact are depicted by the Solid Black column, which shows the changes in the area covered by each vegetation class, the column with inclined lines showing the vegetation class prior to the impact, and the column with horizontal black lines showing the area covered by each vegetation class following the impact

(Ibrahim and Al Maghawry 2022; Terry et al. 2022; Joseph et al. 2023; Al-Awadhi et al. 2024), as our study used higher resolution imagery. It was observed that our study provided the STC impact at detailed levels. The use of low-medium resolution imagery can only provide an overview of such impact, as previous studies have used, which might underestimate the changes in the study area for vegetation and water categories. A similar trend of underestimation was observed in vegetation assessments. Our study stands out by offering a more detailed impact evaluation, incorporating both location-specific and regional-level analyses. Additionally, our use of satellite tasking enabled the timely acquisition of high-resolution imagery, allowing for an early and accurate assessment of the impacts.

3.5 Possible Vulnerable Areas

DEM is a valuable tool for identifying areas that may be susceptible to local flooding during heavy rainfall or flash floods (Anis-Athirah et al. 2021). The results indicate that Al–Khabourah and Al–Suwaiq had high values of R, reaching the highest values of 14 and 15, respectively. The map of the R-index in Al–Khabourah showed that the region near the coast, especially near Wadi Al–Hawasnah and Wadi Bani Omar, is at a high risk of flash flooding because of a significant change in surface elevation. These findings strengthened the results shown in Fig. 16, which highlighted the formation of new water bodies in the wadi after STC impact. The spatial distribution of R in Al–Suwaiq showed that the overall area near the coastline resulted in values varying from 5 to 15, depicting the variation of surface elevation from the surrounding area, leading to a possible flash flood in the area. Figure 18 shows the DEM and R-indices for the study area.

Based on the DEM and R maps, the study constructed hot spots and cold spots analyses in these wilyats using Eqs. 4–6. The analysis helped in the identification and evaluation of the areas that are prone to flash floods caused by TCs. Figure 19 shows the results of the analysis, highlighting these areas. The Hotspot analysis in Al–Khabourah identified the areas that are most likely to be affected in the case of natural hazards, such as the TC impact of rainfall flash floods. Figure 19 (a) shows that Al–Khabourah contains closer clusters of hotspots, especially near the Wadi Al–Hawasnah lagoon, with a confidence of 95–99% in the area, setting the region at greater risk for future flood inundation. In Al–Suwaiq (Fig. 19b), the clusters of hotspots are closer to the coast, which might be prone to flooding when it rains or sea levels rise due to TCs impacts and inflow of water from wadis. As a result of the analysis, hotspot and coldspot cluster information can be used to identify areas that may flood more frequently during intense rainfall. According to hotspot analysis, Al–Khabourah and Al–Suwaiq might be at a higher risk of flooding. As shown by an overlay of the DEM layer over the Hotspot layer, the areas near the coast in Al–Suwaiq at an elevation of 0–10 m, and those near the coastline in Alkhabourah at an elevation of up to 15 m, are at high risk of flooding. In Al–Khabourah (Fig. 19a), a area of 7.1 Square km of the total area is prone to flooding with a 99% confidence value. On the other hand, the hotspot analysis resulted in a total of 0.61 square km of the area near the Suwaiq coastline (Fig. 19b) being prone to flooding with 99% confidence. The insights from Fig. 19 can help policymakers decide where to allocate resources before the impact of the TCs and their landfall in these areas.

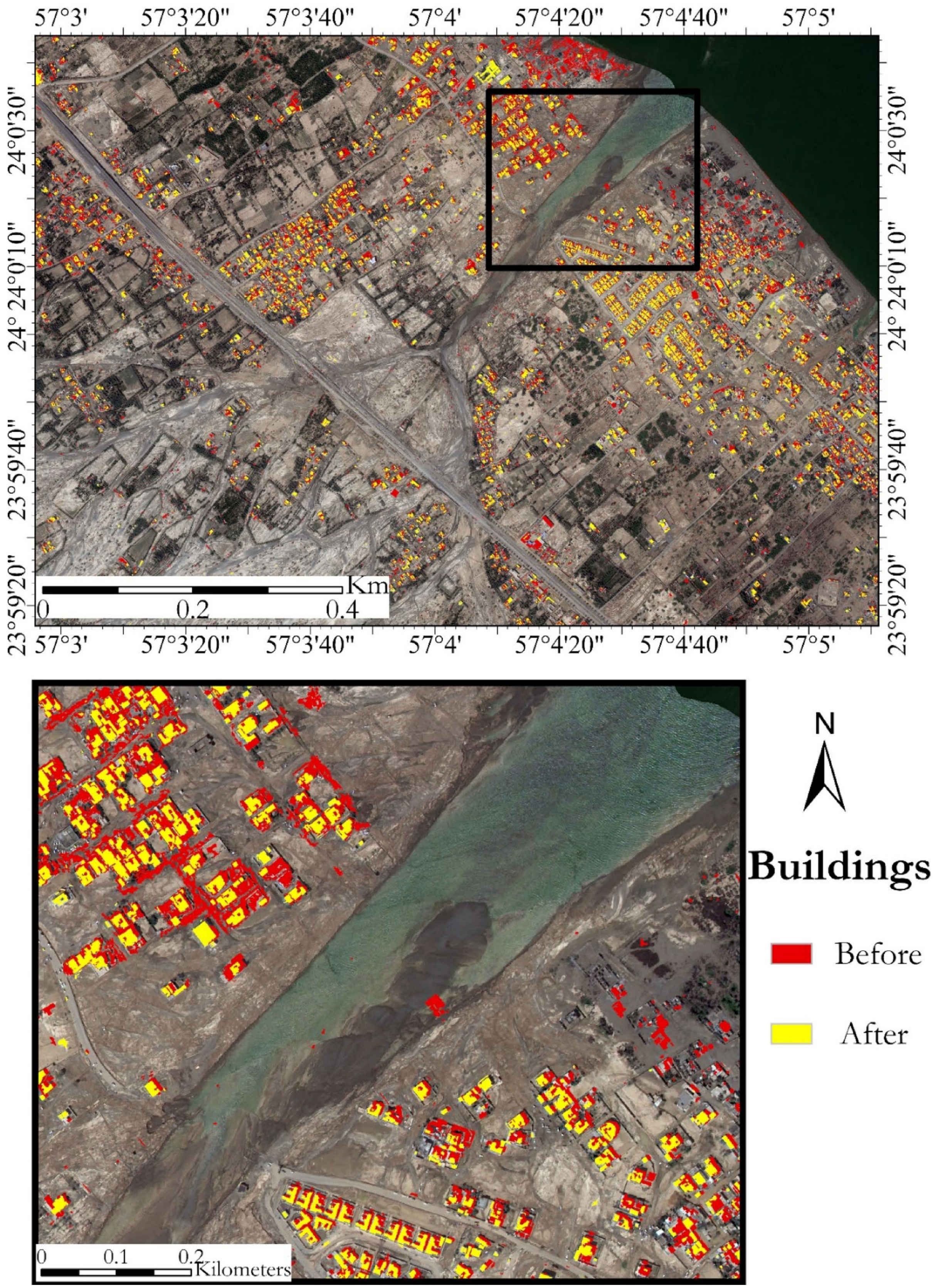

Fig. 17 Impact on the building footprints before and after the STC landfall in Al–Khabourah is shown in red and yellow, respectively

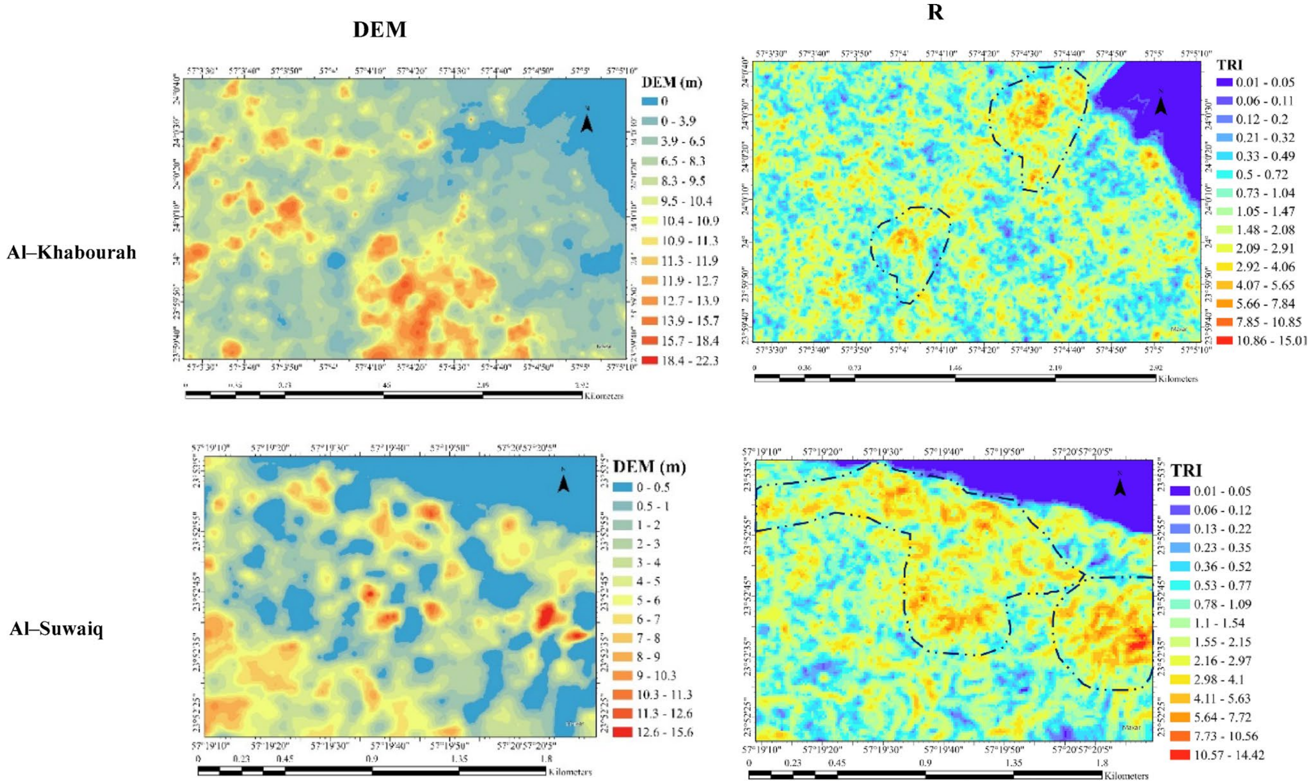

Fig. 18 DEM and TRI for all the wilayats

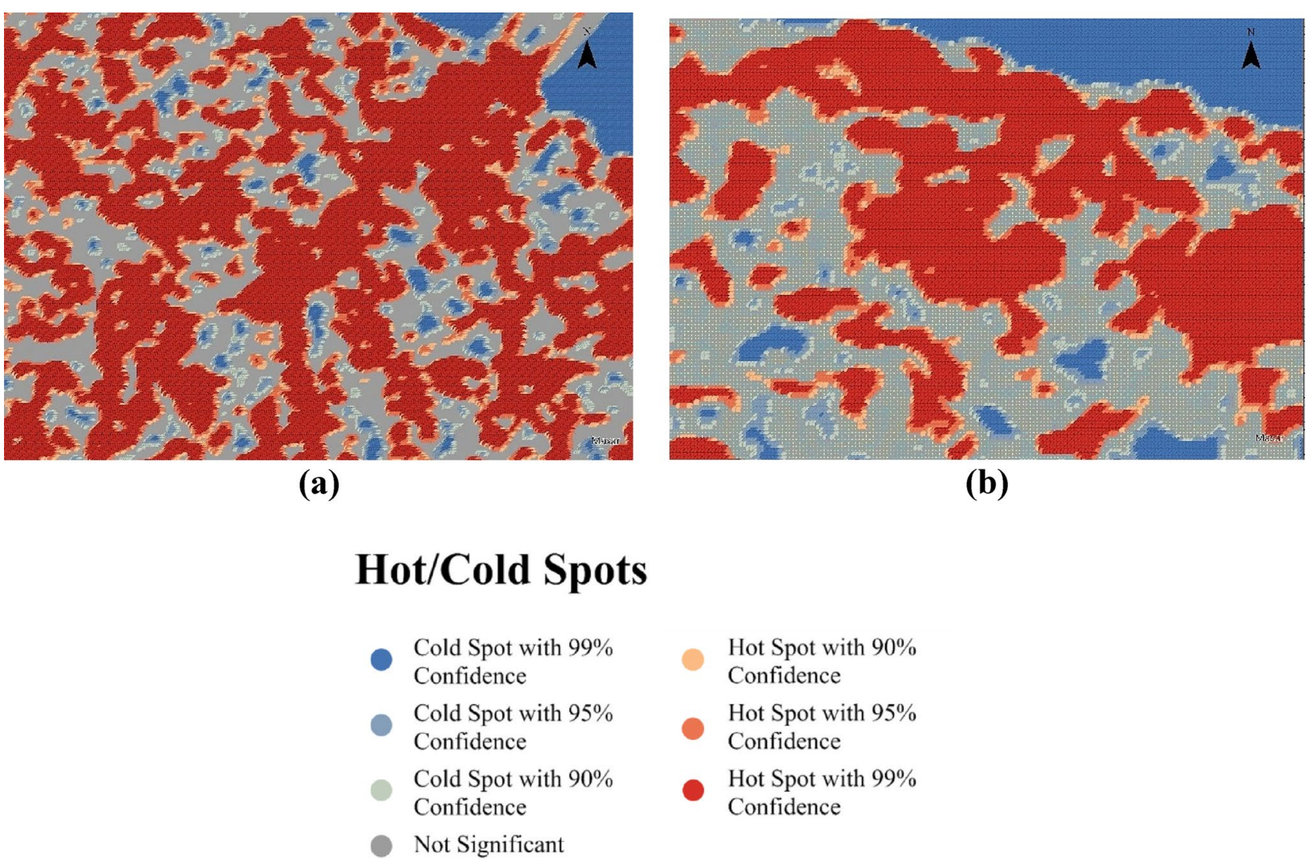

Fig. 19 Hot and Cold spots analysis for (**a**) Al–Khabourah, and (**b**) Al–Suwaiq

3.6 Accuracy Assessment

Figure 20 (a) shows the RGB imagery of Wadi Al–Hawasnah and Wadi Bani Omar Dam on June 31, 2021, with no water stored, whereas Fig. 20 (b) shows the RGB imagery of the dam captured on October 7, 2021, after the STC landfall. On the other hand, Fig. 20 (c) shows the results from the satellite imagery analysis used in this study and confirmed that there was no water detected in the dam before the STC impact while Fig. 20 (d) shows the results of the current research detecting the flow of water in the dam and discharge toward the coastal area (captured on October 7, 2021). This analysis of the dam was cross-examined using data published by the Ministry of Agriculture, Fisheries, and Water Resources, stating that there was no water stored in the dam before the STC impact, and the dam was at its full capacity (3.7 million m^3) on October 4, 2021 (MAFWR_OM, 2021b).

Figure 20 (e) shows the RGB imagery of the roads, vegetation, houses (buildings), and water captured on June 31, 2021, on Google Earth Pro before the STC impact near Wadi Al–Hawasnah Lagoon. Figure 20 (f) shows the impact on the same location of roads, vegetation, houses (buildings), and water captured on October 17, 2021, on Google Earth Pro after the STC impact, resulting in the recorded locations being fully submerged by the water while the building was completely wiped. We found the same results in Fig. 20 (g and h) from our imagery analysis at the same location and found that the ground truthing points of the road, vegetation, and house were completely covered by water after the STC impact. Moreover, the pre–impact imagery used in this study did not detect any water at the ground truth site.

Table 3 shows the results of the accuracy assessment conducted on the imagery with a 5×5 confusion matrix used for deep learning model analysis. The confusion matrix analysis showed that the model was successful in detecting barren, dense, and sparse vegetation with average precision rates of 1, 0.93, and 0.89, respectively. The results showed that the overall accuracy of the model was 94% with a kappa value of 0.92. The accuracy assessment analysis also showed that the highest recall value (1) was observed in water and building detection. Moreover, the overall misclassification rate was 0.06, and the Weighted F1 was 0.84. The confusion matrix analysis showed that 53 TP detections were reported out of 56 geotagged locations of barren land, and 18 TP detections of buildings were reported in the assessment. At the same time, Overall, 125 TP values were recorded from 133 ground-truth points.

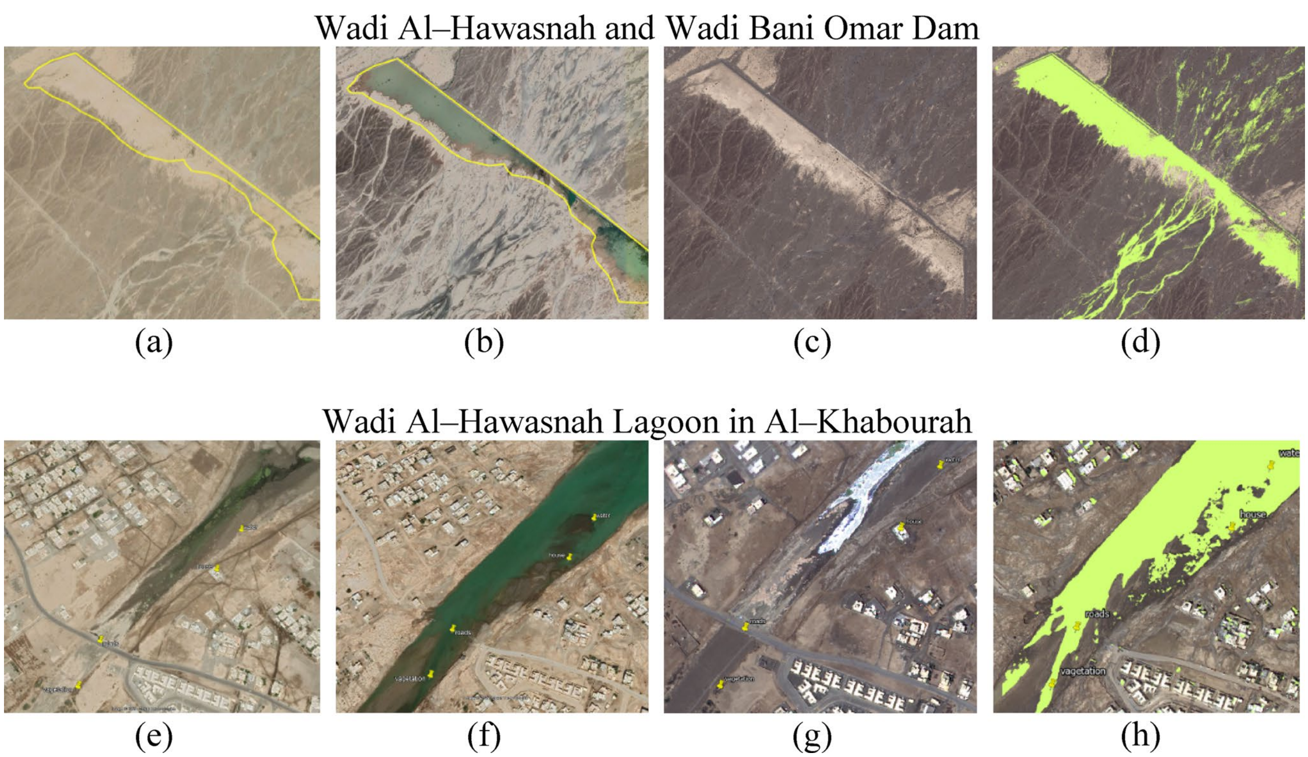

Fig. 20 The geographical locations of the accuracy assessment points used for the accuracy assessment of the study. Where (**a**) shows the RGB imagery of a Dam before STC landfall, (**b**) shows the RGB imagery of the dam after the STC landfall, (**c**) depicts our results that show there was no water detected in the dam before the STC impact, (**d**) depicts our results that show the flow of water in the dam and discharge toward the coastal area, (**e**) shows the RGB imagery of the roads, vegetation, houses (buildings), and water before STC landfall, (**f**) shows the RGB imagery on the same location after the STC landfall, (**g** & **h**) depicts our results in the same location before (g) and (h) after the STC landfall

Table 3 A 5 × 5 confusion matrix analysis

	Barren	Building	Sparse Vegetation	Dense Vegetation	Water	Total
Barren	**53**	0	0	0	0	53
Building	0	**18**	0	2	0	20
Sparse Vegetation	2	0	**34**	2	0	38
Dense Vegetation	0	0	1	**14**	0	15
Water	1	0	0	0	**6**	7
Total	56	18	35	18	6	125/133
	Precision	1-Precision	Recall	1-Recall	F1-score	
Barren	1	0	0.94	0.06	0.95	
Building	0.9	0.1	1	0.01	0.82	
Sparse Vegetation	0.89	0.11	0.97	0.03	0.88	
Dense Vegetation	0.93	0.06	0.78	0.22	0.85	
Water	0.86	0.14	1	0	0.92	
Accuracy	0.94					
Kappa	0.92					
Misclassification Rate	0.06					
Macro-F1	0.92					
Weighted-F1	0.94					

4 Conclusion

On October 3, 2021, the Shaheen tropical cyclone (STC) became the first in 130 years to make a straight landfall in the north of the Al–Batinah Governorate in the Sultanate of Oman after crossing the Oman Sea. This study demonstrates the effective application of artificial intelligence in the form of Multiple Deep learning techniques for detecting and mapping various objects, including vegetation, buildings, and water bodies, in the aftermath of the impact of STC. By leveraging different deep learning models, such as SSD, Mask R–CNN, and YOLOv3, and fine-tuning various parameters, the study achieved high precision in detecting buildings and vegetation, despite challenges such as insufficient training samples for water bodies. The integration of DEM and R maps identified the areas most vulnerable to flooding, reinforcing the importance of predictive tools in natural climate disaster management. The study focused on the holistic influence of STC on the region's urban, vegetation, and biodiversity changes using a deep learning algorithm that yielded an overall accuracy of 94% with a kappa value of 0.92. The analysis found that Al–Suwaiq and Al–Khabourah were directly hit by the STC landfall, where Al–Khabourah experienced the maximum cumulative rainfall (369 mm), followed by Al–Suwaiq (300 mm) and Saham (214 mm). The analysis revealed that 85.8 ha (51.3%) of the dense vegetation was destroyed in Al–Khabourah. Moreover, 153.2 ha (18.9%) of the sparse vegetation was destroyed after the STC impact. The investigation for vegetation revealed that Al–Suwaiq was the most impacted wilayat, with 1713.9 ha (67.2%) of dense vegetation, 3160 ha (55.5%) of shrubs and grasses, and 609.8 ha (16.6%) of sparse vegetation fully devastated by the STC impact. On the other hand, the post–impact analysis revealed the formation of new water bodies, as well as an increase in the size of existing water bodies in Al–Khabourah (496.82 ha) and Al–Suwaiq (180.8 ha). The results from this study showed damage to 32% (42.73 ha) of buildings in Al–Khabourah, and 67.5% (6.4 ha) of the fishermen's structures near the beach were destroyed due to high winds and water surges. This study will also assist the concerned authorities in anticipating similar TCs in unexpected regions. The emergency response team can incorporate the local administration from the areas identified from the hotspot and DEM results to develop a framework of essential measures in the case of extensive rainfalls and possible floods. These measures ensure the cleaning and monitoring of wadis with the help of municipal cooperation to make sure that the Wadi can lead to a safe water discharge. The building of the new agricultural or residential structure must be addressed by the housing and agricultural sectors following the Oman National Spatial Strategy 2040, particularly in coastal areas, close to Wadi Ways, or at the intersection of waterways (not even within a buffer zone of 50 m). In order to prevent damage from debris in coastal areas, the temporary residential structure must also adhere to the authorities' direction of a 50–300 m (depending upon coastal zones) setback from the highest tidal mark. These insights can support government agencies and landowners in developing more effective pre–impact and post–impact planning and climate resilience strategies, especially in urban and coastal regions. The suggested methodology can be extended to investigate different outcomes of natural climate change disasters at different scales and periods, in collaboration with numerous stakeholders from the private sector, civil society, and government institutions.

Acknowledgements This research was supported by His Majesty's strategic fund at Sultan Qaboos University.

Author Contributions Y.M., A.A., and K.P. developed and validated this study. Y.M., A.A., and M.A. analyzed the results and wrote the initial draft of the manuscript. Y.M., A.A., M.A., F.M., K.P., and T.A. provided input and reviewed the manuscript. All authors have read and approved the final manuscript.

Funding Logistics support and contributions were provided under an SQU grant with the code SR/DVC/GISC/20/01.

Data Availability The set of data generated and/or analyzed during the present study is available through the corresponding author upon reasonable request.

Declarations

Conflict of interest The authors declare no conflict of interest.

References

Al Ruheili A, Dahm R, Radke J (2019) Wadi flood impact assessment of the 2002 cyclonic storm in Dhofar, Oman under present and future sea level conditions. J Arid Environ Jun 1:165:73–80. https://doi.org/10.1016/j.jaridenv.2019.04.002

Al-Awadhi T, Abdullah M, Al-Ali Z, Abulibdeh A, Al-Barwani M, Al Nasiri N, Al-Naabi S, Mohan M (2024) Navigating cyclone threats: a forecast approach using water streams' physical characteristics as an indicator to predict high risk potential areas in the Sultanate of Oman. Earth Syst Environ 2024:1–13. https://doi.org/10.1007/S41748-024-00392-2

Al-Hatrushi S (2013) Monitoring of the shoreline change using remote sensing and GIS: A case study of al-Hawasnah tidal inlet, al Batinah coast, Sultanate of Oman. Arab J Geosci 6:1479–1484. https://doi.org/10.1007/s12517-011-0424-2

Al-Hatrushi S, Al-Alawi H (2011) Evaluating the impact of flood hazard caused by tropical cyclones on land use using remote sensing and GIS in Wadi Uday: Sultanate of Oman. In Proceedings of the 34th International Symposium on Remote Sensing of Environment-The GEOSS Era: Towards Operational Environmental Monitoring, Sidney, NSW, Australia pp. 10–15

Al-Kindi KM, Al Nadhairi R, Al Akhzami S (2023) Dynamic change in normalised vegetation index (NDVI) from 2015 to 2021 in Dhofar, Southern Oman in response to the climate change. Agric 13(3):592. https://doi.org/10.3390/agriculture13030592

Al-Manji S, Mitchell G, Al Ruheili A (2021) Arabian sea tropical cyclones: A Spatio-Temporal analysis in support of natural hazard risk. Agrometeorol 19:145. https://doi.org/10.5772/intechopen.96961

Al-Mulla Y, Al-Ruheili A, Al-Lawati A, Parimi K, Ali A, Al-Sadi N, Al-Harrasi F (2022) Assessment of urban expansion's impact on changes in vegetation patterns in Dhofar, Oman, using remote sensing and GIS techniques. IEEE Access 10:86782–86792. https://doi.org/10.1109/access.2022.3198942

Al-Zadjali S, Al-Rawahi Z, Al-Brashdi H (2021) The impact of tropical cyclones in premonsoonal season on local convection over the Al-Hajar mountains in Oman during 2007–2018. Adv Meteorol 2021(1):5543205. https://doi.org/10.1155/2021/5543205

Ali A, Al-Mulla YA, Charabi Y, Al-Wardy M, Al-Rawas G (2021) Use of multispectral and thermal satellite imagery to determine crop water requirements using SEBAL, METRIC, and SWAP models in hot and hyper-arid Oman. Arab J Geosci 14(7):634. https://doi.org/10.1007/s12517-021-06948-0

AlRuheili AM (2022) A Tale of shaheen's cyclone consequences in al Khaboura City. Oman Water 14(3):340. https://doi.org/10.3390/w14030340

Andreou GM, Westley K, Huigens HO, Blue L (2022) Exploring the impact of tropical cyclones on oman's maritime cultural heritage through the lens of Al-Baleed, Salalah (Dhofar Governorate). J Marit Archaeol 17(3):465–486. https://doi.org/10.1007/s11457-022-09333-4

Anis-Athirah BN, Mohd-Fariz AR, Bam HNR, Majid S, Muhammad M, Jemali NJN (2021) Delineation of flood-prone areas using digital elevation model (DEM) in Kuala Krai, Kelantan. IOP Conf Ser: Earth Environ Sci 842(1):012045. https://doi.org/10.1088/1755-1315/842/1/012045

Baek Y-H, Moon I-J, Im J, Lee J (2022) A novel tropical cyclone size Estimation model based on a convolutional neural network using geostationary satellite imagery. Remote Sens 14:426. https://doi.org/10.3390/rs14020426

Banan-Dallalian M, Shokatian-Beiragh M, Golshani A, Mojtahedi A, Lotfollahi-Yaghin MA, Akib S (2021) Study of the effect of an environmentally friendly flood risk reduction approach on the Oman coastlines during the Gonu tropical cyclone (Case study: the coastline of Sur). Eng 2:141–155. https://doi.org/10.3390/eng2020010

Behera MD, Prakash J, Paramanik S, Mudi S, Dash J, Varghese R, Roy PS, Abhilash PC, Gupta AK, Srivastava PK (2022) Assessment of tropical cyclone Amphan affected inundation areas using sentinel-1 satellite data. Trop Ecol 63:9–19. https://doi.org/10.1007/s42965-021-00187-w

Berezina P, Liu D (2022) Hurricane damage assessment using coupled convolutional neural networks: a case study of hurricane Michael. Geomat Nat Hazards Risk 13:414–431. https://doi.org/10.1080/19475705.2022.2030414

Charrua AB, Padmanaban R, Cabral P, Bandeira S, Romeiras MM (2021) Impacts of the tropical cyclone Idai in mozambique: A Multi-Temporal Landsat satellite imagery analysis. Remote Sens 13:201. https://doi.org/10.3390/rs13020201

Chen B, Kuo Y, Huang T (2023) A deep learning ensemble approach for predicting tropical cyclone rapid intensification. Atmos Sci Lett. https://doi.org/10.1002/asl.1151

Civil Aviation Authority (CAA) (2025) Preliminary Report on Tropical Cyclone 1–4 October 2021 [internet]; Department of Research and Development: Muscat, Oman, 2021 Avaialable from: https://met.caa.gov.om/tropical-cyclone-shaheen-1-4-oct-2021/. Accessed 5 July

Cortés-Ramos J, Farfán LM, Herrera-Cervantes H (2020) Assessment of tropical cyclone damage on dry forests using multispectral

remote sensing: the case of Baja California Sur, Mexico. J Arid Environ 178:104171. https://doi.org/10.1016/j.jaridenv.2020.104171
Das S, Ghosh T (2024) Identifying the gaps in cyclone vulnerability mitigation in the Indian Sundarban using AHP based multi criteria decision analysis (MCDA) and GIS techniques: tool for the policy makers. Earth Syst Environ. https://doi.org/10.1007/s41748-024-00486-x
Delaporte B, Ibanez T, Despinoy M, Mangeas M, Menkes C (2022) Tropical cyclone impact and forest resilience in the Southwestern Pacific. Remote Sens 14:1245. https://doi.org/10.3390/rs14051245
Deutsche W (2021) Cyclone Shaheen Leaves Several Dead in Oman [internet]. Deutsche Welle. Available on https://www.dw.com/en/cyclone-shaheen-leaves-several-dead-in-oman/a-59390343. Accessed 25 September 2025
Dong P, Lian J, Yu H, Pan J, Zhang Y, Chen G (2022) Tropical cyclone track prediction with an Encoding-to-Forecasting deep learning model. Weather Forecast 37:971–987. https://doi.org/10.1175/waf-d-21-0116.1
Erick BS (2025) Tropical cyclones - statistics & facts [internet]. Statista [Cited on 2025 April 3] Available from: https://www.statista.com/topics/11168/tropical-cyclones/#topicOverview
ESRI (2023a) Hot Spot Analysis (Getis-Ord Gi*) (Spatial Statistics)—ArcGIS Pro | Documentation. https://pro.arcgis.com/en/pro-app/latest/tool-reference/spatial-statistics/hot-spot-analysis.htm
ESRI (2023b) How Hot Spot Analysis (Getis-Ord Gi*) works—ArcGIS Pro | Documentation. https://pro.arcgis.com/en/pro-app/latest/tool-reference/spatial-statistics/h-how-hot-spot-analysis-getis-ord-gi-spatial-stati.htm
Feehan CJ, Filbee-Dexter K, Thomsen MS, Wernberg T, Miles T (2024) Ecosystem damage by increasing tropical cyclones. Commun Earth Environ 5(1):674. https://doi.org/10.1038/s43247-024-01853-2
Feng Y, Negrón-Juárez RI, Chambers JQ (2021) Multi-cyclone analysis and machine learning model implications of cyclone effects on forests. Int J Appl Earth Obs Geoinf 103:102528. https://doi.org/10.1016/j.jag.2021.102528
Fisker P, Malmgren-Hansen D, Sohnesen TP (2021) Remote sensing of urban cyclone impact and resilience: evidence from Idai. WIDER Working Paper. https://doi.org/10.35188/unu-wider/2021/029-0
Fritz HM, Blount C, Albusaidi FB, Al-Harthy AHM (2010) Cyclone Gonu storm surge in the Gulf of Oman. Indian ocean tropical cyclones and climate change. Springer, pp 255–263. https://doi.org/10.1007/978-90-481-3109-9_30
Gahtan J, Knapp KR, Schreck CJ, Diamond HJ, Kossin JP, Kruk MC (2024) International Best Track Archive for Climate Stewardship (IBTrACS) Project, Version 4r01. [all subset used]. NOAA National Centers for Environmental Information. https://doi.org/10.25921/82ty-9e16. Accessed 29 April 2024
Gao B (1996) NDWI—A normalized difference water index for remote sensing of vegetation liquid water from space. Remote Sens Environ 58:257–266. https://doi.org/10.1016/s0034-4257(96)00067-3
Haque MN, Ashfaqul AAM, Alam KS (2022) Deep Learning Techniques in Cyclone Detection with Cyclone Eye Localization Based on Satellite Images. In Arefin MS, Kaiser MS, Bandyopadhyay A, Ahad MAR, Ra, K (eds) Proceedings of the International Conference on Big Data, IoT, and Machine Learning. Lecture Notes on Data Engineering and Communications Technologies 95. Springer, Singapore. https://doi.org/10.1007/978-981-16-6636-0_35
Hassan MM, Ash K, Abedin J, Paul BK, Southworth J (2020) A quantitative framework for analyzing Spatial dynamics of flood events: A case study of super cyclone Amphan. Remote Sens 12(20):3454. https://doi.org/10.3390/rs12203454
He K, Gkioxari G, Dollar P, Girshick R (2020) Mask R-CNN. IEEE Trans Pattern Anal Mach Intell 42(2):386–397. https://doi.org/10.1109/TPAMI.2018.2844175
Hong X, Cui X-Z, Lyu M-Z, Kong F (2025) A multiscale framework for the risk analysis of urban Building envelope systems subject to windborne debris considering the directional effect of tropical cyclones. J Wind Eng Ind Aerodyn 265:106160. https://doi.org/10.1016/j.jweia.2025.106160
Hoque MAA, Phinn S, Roelfsema C, Childs I (2016) Assessing tropical cyclone impacts using object-based moderate Spatial resolution image analysis: a case study in Bangladesh. Int J Remote Sens 37(22):5320–5343. https://doi.org/10.1080/01431161.2016.1239286
Hoque MAA, Sardar ML, Sami MS, Roy S, Mukul SA, Pradhan B (2024) Mapping tropical cyclone risks in coastal bangladesh: an integrated Geospatial approach. Earth Syst Environ 9:1353–1370. https://doi.org/10.1007/s41748-024-00547-1
Hungwe M-G, Gumindoga W, Manuel Baez Villanueva O, Rwasoka DT (2024) Comparative analysis of the variability and impacts of tropical cyclones in flood-prone areas of Zimbabwe. Front Clim. https://doi.org/10.3389/fclim.2024.1291751
Ibrahim OR, Al Maghawry S (2022) Review on cyclone Shaheen in the Sultanate of Oman. Arab J Geosci. https://doi.org/10.1007/s12517-022-10118-1
Jiang W, Hu G, Wu T, Liu L, Kim B, Xiao Y, Duan Z (2023) DMANet_KF: tropical cyclone intensity Estimation based on deep learning and Kalman filter from multispectral infrared images. IEEE J Sel Top Appl Earth Observations Remote Sens 16:4469–4483. https://doi.org/10.1109/jstars.2023.3273232
Joseph MA, Natarajan J, Al Farsi TK, Al Saifi AZM, Al Saidi WK, Al Jassassi OA, Al Mukhaini HM (2023) The impact of the 2021 cyclone Shaheen on the mental health of affected Omanis. Oman Med J 38:e483–e483. https://doi.org/10.5001/omj.2023.62
Kai KH, Shaghude YW, Kijazi AL, Uiso CB (2021) The influence of tropical cyclones to the plant productivity indices along the Coast of Tanzania. ACS 11:589–613. https://doi.org/10.4236/acs.2021.113036
Kaspi M, Kuleshov Y (2023) Flood hazard assessment in Australian tropical Cyclone-Prone regions. Climate 11:229. https://doi.org/10.3390/cli11110229
Kathuria A (2018) What's New in YOLO v3? Medium. 23 April https://medium.com/towards-data-science/yolo-v3-object-detection-53fb7d3bfe6b. Accessed 3 April 2025
Kaur S, Gupta S, Singh S (2021) Hurricane damage detection using machine learning and deep learning techniques: A review. IOP Conf Ser: Mater Sci Eng 1022:012035. https://doi.org/10.1088/1757-899x/1022/1/012035
Knutson TR, McBride JL, Chan J, Emanuel K, Holland G, Landsea C, Held I, Kossin JP, Srivastava AK, Sugi M (2010) Tropical cyclones and climate change. Nat Geosci 3:157–163. https://doi.org/10.1038/ngeo779
Kropf CM, Vaterlaus L, Bresch DN, Pellissier L (2025) Tropical cyclone risk for global ecosystems in a changing climate. Nat Clim Chang 15:92–100. https://doi.org/10.1038/s41558-024-02194-w
Kumar R, Rani S, Maharana P (2021) Assessing the impacts of Amphan cyclone over West Bengal, india: a multi-sensor approach. Environ Monit Assess. https://doi.org/10.1007/s10661-021-09071-5
Li Y, Hu W, Dong H, Zhang X (2019) Building damage detection from Post-Event aerial imagery using single shot multibox detector. Appl Sci 9:1128. https://doi.org/10.3390/app9061128
Lin YC, Feng SN, Lai CY, Tseng HT, Huang CW (2023) Applying deep learning to predict SST variation and tropical cyclone

patterns that influence coral bleaching. Ecol Inf 77:102261. https://doi.org/10.1016/j.ecoinf.2023.102261
Liu W, Anguelov D, Erhan D, Szegedy C, Reed S, Fu CY, Berg AC (2015) SSD: single shot multibox detector. ArXiv. https://doi.org/10.48550/ARXIV.1512.02325
Liu W, Anguelov D, Erhan D, Szegedy C, Reed S, Fu CY, Berg AC (2016) SSD: single shot multibox detector. Lect Notes Comput Sci 21–37. https://doi.org/10.1007/978-3-319-46448-0_2
Lung L-W, Wang Y-R (2023) Applying deep learning and single shot detection in construction site image recognition. Buildings 13:1074. https://doi.org/10.3390/buildings13041074
Luo H, Wu J (2022) Exploring the Spatial pattern of damage caused by typhoon meranti on the urban green space on Xiamen Island. Nat Env Poll Tech 21:315–319. https://doi.org/10.46488/nept.2022.v21i01.038
MAFWR_OM a Rainfall distribution over a number of governorates of the Sultanate during the period from October 2 to 4, 2021 (until 8:00 AM). X. 4 October 2021. https://x.com/MAFWR_OM/status/1444918206892847104. Accessed 28 September 2025
MAFWR_OM b The amount of water stored in dams. X. 4 October 2021. https://x.com/MAFWR_OM/status/1444987407284252672. Accessed 28 September 2025
Maha Arachchige S, Pradhan B (2025) AI Meets the eye of the storm: machine Learning-Driven insights for hurricane damage risk assessment in Florida. Earth Syst Environ 9:2143–2163. https://doi.org/10.1007/s41748-025-00571-9
Mandal MSH, Hosaka T (2020) Assessing cyclone disturbances (1988–2016) in the sundarbans Mangrove forests using Landsat and Google Earth engine. Nat Hazards 102:133–150. https://doi.org/10.1007/s11069-020-03914-z
Mansour S (2019) Geospatial modelling of tropical cyclone risks to the Southern Oman Coasts. Int J Disaster Risk Reduct 40:101151. https://doi.org/10.1016/j.ijdrr.2019.101151
Mansour S, Alahmadi M, Darby S, Leyland J, Atkinson PM (2023) Geospatial modelling of post-cyclone Shaheen recovery using nighttime light data and MGWR. Int J Disaster Risk Reduct 93:103761. https://doi.org/10.1016/j.ijdrr.2023.103761
Mishra M, Acharyya T, Halder B, Santos CAG, Silva RM da, Rout NR, Bhattacharyya D (2024) Impact assessment of cyclone Yaas on the Mangrove forest area in the Bhitarkanika National park (India). J Mar Syst 242:103947. https://doi.org/10.1016/j.jmarsys.2023.103947
Müller T, Friesen J, Weise SM, Al Abri O, Bait Said ABA, Michelsen N (2020) Stable isotope composition of cyclone Mekunu Rainfall, Southern Oman. https://doi.org/10.1029/2020wr027644. Water Resources Research
Murray VJ, Abrahams C, Abdallah K, Ahmed L et al (2020) Hazard Information Profiles: Supplement to UNDRR-ISC Hazard Definition & Classification Review – Technical Report. Geneva, Switzerland; Paris, France: UNDDR
NASA (2024) Worldview data. Acquired between 2 and 4 October 2021 for cyclone Shaheen impact area. https://worldview.earthdata.nasa.gov/
Nasrin T, Ramiz M, Sarif MN, Hashim M, Siddiqui MA, Siddiqui L, Mohibul S, Mankotia S (2023) Modeling of impact assessment of super cyclone Amphan with machine learning algorithms in Sundarban biosphere Reserve, India. Nat Hazards 117:1945–1968. https://doi.org/10.1007/s11069-023-05935-w
Ningsih NS, Hanifah F, Tanjung TS, Yani LF, Azhar MA (2020) The effect of tropical cyclone Nicholas (11–20 February 2008) on sea level anomalies in Indonesian waters. JMSE 8:948. https://doi.org/10.3390/jmse8110948
Observer O (2021) The extent of damages caused by cyclone Shaheen in al Suwaiq area is beyond our imagination. X. https://x.com/OmanObserver/status/1444921537358962688. Accessed 28 September 2025
Okolie C, Mills J, Adeleke A, Smit J (2023) Digital elevation model correction in urban areas using extreme gradient boosting, land cover and terrain parameters. https://doi.org/10.48550/ARXIV.2308.06545
Olorunshola O, Jemitola P, Ademuwagun A, Nile (2023) J Eng Appl Sci 1(1):70–80. https://doi.org/10.5455/NJEAS.150264
Phiri D, Simwanda M, Nyirenda V (2020) Mapping the impacts of cyclone Idai in Mozambique using Sentinel-2 and OBIA approach. South Afr Geogr J 103:237–258. https://doi.org/10.1080/03736245.2020.1740104
Prakash S, Varghese A, Amrutha AS, Baiju KR (2023) Assessment of ecological disturbance on Indian sundarbans with special reference to Amphan cyclone by using Geospatial technology. J Geospat Surv 3:26–32. https://doi.org/10.4038/jgs.v3i1.47
Redmon J, Farhadi A (2018) Yolov3: An incremental improvement. arXiv preprint http://arxiv.org/abs/1804.02767
Riley SJ, DeGloria SD, Elliot R (1999) Index that quantifies topographic heterogeneity. Intermt J Sci 5(1–4):23–27
Rochmadi S (2023) Review of elevation data derived from Google Earth. AIP Conf Proc 2791(1):030012. https://doi.org/10.1063/5.0128832
Shamsuzzoha M, Noguchi R, Ahamed T (2021) Damaged area assessment of cultivated agricultural lands affected by cyclone Bulbul in coastal region of Bangladesh using Landsat 8 OLI and TIRS datasets. Remote Sens Appl Soc Environ 23:100523. https://doi.org/10.1016/j.rsase.2021.100523
Srivastava G, Kavitha V, Vimaladevi M, Parthiban N (2022) The hydrological impact of tropical cyclones on soil moisture using a sensor based hybrid deep learning model. Acta Geophys 70:2933–2951. https://doi.org/10.1007/s11600-022-00942-0
Terry J, Al Ruheili A, Boldi R, Gienko G, Stahl H (2022) Cyclone-Shaheen: the exceptional tropical cyclone of October 2021 in the Gulf of Oman. Weather 77:364–370. https://doi.org/10.1002/wea.4193
Times of Oman (2021) Cyclone Shaheen: Volunteer drive to help clean homes in Oman, 7 October. Available at: https://timesofoman.com/article/107716-cyclone-shaheen-volunteer-drive-to-help-clean-homes-in-oman (Accessed: 11 October 2025)
Tomaszewski B (2020) Geographic information systems (GIS) for disaster management, 2nd edn. Routledge, New York. https://doi.org/10.4324/9781351034869
Trevisani S, Teza G, Guth PL (2023) Hacking the topographic ruggedness index. Geomorphol 439:108838. https://doi.org/10.1016/j.geomorph.2023.108838
Viraktamath DS, Navalgi P, Neelopant A (2021) Comparison of YOLOv3 and SSD algorithms. Int J Eng Res Technol 10(2):193–196
Xie M, Li Y, Dong S (2022) A Deep-Learning-Based fusion approach for global cyclone detection using multiple remote sensing data. IEEE J Sel Top Appl Earth Obs Remote Sens 15:9613–9622. https://doi.org/10.1109/jstars.2022.3219809
Zhang X, Wang Y, Jiang H, Wang X (2013) Remote-sensing assessment of forest damage by typhoon Saomai and its related factors at landscape scale. Int J Remote Sens 34:7874–7886. https://doi.org/10.1080/01431161.2013.827344
Zhang CJ, Wang XJ, Ma LM, Lu XQ (2021) Tropical cyclone intensity classification and Estimation using infrared satellite images with deep learning. IEEE J Sel Top Appl Earth Obs Remote Sens 14:2070–2086. https://doi.org/10.1109/JSTARS.2021.3050767
Zhao L, Li S (2020) Object detection algorithm based on improved YOLOv3. Electron 9(3):537. https://doi.org/10.3390/electronics9030537

Zhou M, Kuang Y, Ruan Z, Xie M (2021) Geospatial modeling of the tropical cyclone risk in the Guangdong Province, China. Geomat Nat Hazards Risk 12(1):2931–2955. https://doi.org/10.1080/19475705.2021.1972046

Zhuo JY, Tan ZM (2021) Physics-augmented deep learning to improve tropical cyclone intensity and size Estimation from satellite imagery. Mon Wea Rev 149(7):2097–2113. https://doi.org/10.1175/MWR-D-20-0333.1